

## Next-Generation Materials Discovery Using DFT: Functional Innovation, Solar Energy, Catalysis, and Eco Toxicity Modelling

Muhammad Tayyab Iqbal<sup>1</sup>, Saman Saecda<sup>2</sup>, Tehleel Zahra<sup>3</sup>, Zeeshan Umar<sup>4</sup>, Waheed Zaman Khan<sup>5\*</sup>, Muhammad Adnan<sup>6</sup>, Hasan Raza<sup>7</sup>, Ghafar Ali Shah<sup>8</sup>, Muhammad Toffique<sup>9</sup>

<sup>1</sup>Department of Physics, University of Agriculture, Faisalabad, Punjab, Pakistan

<sup>2</sup>Department of Chemistry, University of Management and Technology, Lahore, Punjab, Pakistan

<sup>3</sup>Department of Chemistry, University of Agriculture, Faisalabad, Punjab, Pakistan

<sup>4</sup>School of Mechanics and Engineering Sciences, Hohai University, Nanjing 211100, China

<sup>5</sup>Department of Physics, Division of Science and Technology, University of Education, Lahore, Punjab 54770, Pakistan

<sup>6</sup>Department of Chemical, Polymer and Composite Materials Engineering, University of Engineering and Technology, Lahore, Punjab, Pakistan

<sup>7</sup>Department of Physics, University of Education, Lahore (Faisalabad Campus), Punjab, Pakistan

<sup>8</sup>Institute of Chemical Sciences, University of Swat, Swat, Khyber Pakhtunkhwa, Pakistan

<sup>9</sup>Department of Mechanical Engineering Technology, The University of Lahore, Lahore, Punjab, Pakistan

DOI: <https://doi.org/10.36347/sjet.2025.v13i07.003>

| Received: 29.04.2025 | Accepted: 03.06.2025 | Published: 05.07.2025

\*Corresponding author: Waheed Zaman Khan

Department of Physics, Division of Science and Technology, University of Education, Lahore, Punjab 54770, Pakistan

### Abstract

### Review Article

Providing calculations with high precision and on the atom scale of materials' electronic, optical and structural characteristics, DFT has fundamentally changed the field of computational materials science. This review provides an extensive review of DFT's development from early local and semi-local functionals (LDA, GGA) through more sophisticated hybrid (HSE06, B3LYP) and meta-GGA (SCAN, MVS) methods. In addition, the review includes state-of-the-art beyond-DFT methods such as TDDFT, the GW approximation, and the Bethe–Salpeter Equation (BSE) necessary for excited states and optoelectronic behavior understanding and predictions. The combination of machine learning techniques and DFT is studied as a promising method of accelerating the discovery of new materials. A major emphasis is placed on modelling perovskite, silicon-based, and thin-film solar cells (CIGS, CZTS), using DFT to manage band gaps. The importance of the theory in increasing charge transport, reducing the rates of recombination and increasing power conversion efficiency are emphasized. In the field of environmental sustainability, DFT is applied to design efficient photocatalysts for wastewater purification and hydrogen production to gain knowledge on the process of pollutants decomposition and the toxicity of emerging compounds. DFT-derived data supports lifecycle assessments to shape eco-design in photovoltaic systems, as well as decisions about photovoltaic recyclability, energy payback, and environmental sustainability. This review brings forth DFT's key role in pushing for breakthrough development for energy, environment, and nanotechnological sectors. Indeed, based on quantum simulations, as well as on the evidence and data-backed approaches, DFT continues to widen the field of sustainable material science and clean energy design.

**Keywords:** Density Functional Theory (DFT), Hybrid and Meta-GGA Functionals, Time-Dependent DFT (TDDFT), GW-BSE Calculations, Perovskite Solar Cells, Charge Transport and Recombination, Photocatalysis and Water Treatment, Band Structure Engineering, Nanomaterials and Quantum Dots, Environmental Toxicity Modeling, Lifecycle Assessment Machine Learning in Materials Design.

Copyright © 2025 The Author(s): This is an open-access article distributed under the terms of the Creative Commons Attribution 4.0 International License (CC BY-NC 4.0) which permits unrestricted use, distribution, and reproduction in any medium for non-commercial use provided the original author and source are credited.

## 1. INTRODUCTION

### 1.1. Introduction to Density Functional Theory (DFT)

Density Functional Theory (DFT) has emerged as a fundamental pillar in quantum mechanical modelling, enabling the accurate prediction of electronic properties in atoms, molecules, and condensed matter

systems. Initially developed from the Thomas–Fermi model, the theoretical framework of DFT underwent a significant transformation with the establishment of the Hohenberg–Kohn theorems. These theorems confirmed that all ground-state properties of a many-electron system could be described as functionals of the electron density, thus shifting the variational principle from

wavefunctions to electron densities (Chen, Xu, & Chen, 2020; Helgaker & Teale, 2022).

Kohn and Sham introduced a practical approach that replaces the complex many-body system with non-interacting electrons subject to an effective potential to render the theory computationally feasible. This simplification, expressed through the Kohn–Sham equations, preserved computational efficiency without compromising accuracy, especially for ground-state calculations (Iqbal *et al.*, 2021). Central to this approach is the exchange–correlation functional, which captures electron–electron interactions beyond the classical mean-field approximation. Over the years, several approximations for this functional—most notably the Local Density Approximation (LDA) and the Generalised Gradient Approximation (GGA)—have been developed, each balancing accuracy with computational demand (Penz *et al.*, 2022). For systems exhibiting strong correlation effects, such as transition metal oxides, the DFT+U method provides corrective enhancements by addressing the limitations of standard functionals (Cimpoesu & Putz, 2018). More recently, novel extensions and enhancements of DFT have been explored. Entropy-based DFT frameworks have incorporated thermodynamic principles to extend the applicability of DFT to finite-temperature systems through entropy maximisation (Yousefi & Caticha, 2022). Concurrently, machine learning techniques are being utilised to optimise the performance of exchange–correlation functionals, offering improved predictive capabilities and transferability across different chemical systems (Nagai, Akashi, & Sugino, 2019).

DFT plays an indispensable role in computational materials science, where it facilitates the first-principles prediction of a broad range of physical properties—such as electronic band structures, density of states, optical responses, and mechanical characteristics—without the need for empirical data (Singh & Harbola, 2021; Hu & Chen, 2021). Its application spans metals, semiconductors, and emerging nanomaterials. For example, titanium-based and Heusler alloys have been extensively studied using DFT due to their tunable magnetic, mechanical, and structural properties. These materials are crucial in aerospace, spintronics, and biomedical engineering (Kapil, Shukla, & Pathak, 2020). DFT simulations help elucidate phase stability, electronic configurations, and phase transition mechanisms, thereby accelerating experimental advancements. Additionally, DFT has proven highly effective in studying surfaces and interfaces at the atomic scale, which is critical for applications in catalysis, corrosion resistance, and nanosensor development (Penz *et al.*, 2022). With the advent of linear-scaling algorithms, DFT can now handle large systems, enabling investigations into polymers, biomolecular systems, and complex hybrid frameworks (Hu & Chen, 2021).

In the domains of energy and environmental sustainability, DFT has established itself as a critical tool for designing and optimising materials used in energy conversion and storage devices, including lithium-ion batteries, perovskite solar cells, and fuel cells (Iqbal *et al.*, 2021). It assists in tailoring band gaps for efficient photovoltaic absorption and identifying host materials with high ion mobility and storage capacity. From an environmental perspective, DFT is extensively used to understand and enhance catalytic mechanisms aimed at reducing industrial pollutants. For example, it aids in modelling the interaction between contaminants and adsorbents in water purification and analysing reaction pathways in catalytic converters (Cimpoesu & Putz, 2018).

Advanced materials such as perovskites and metal-organic frameworks (MOFs) are actively being explored for applications like carbon capture, hydrogen storage, and thermoelectric energy conversion. DFT provides crucial insights into their structural and electronic behaviours, guiding the design of next-generation sustainable technologies (Kapil, Shukla, & Pathak, 2020). As the global scientific community intensifies efforts toward cleaner energy and greener industrial processes, DFT will continue to be central to the discovery, design, and development of novel materials with minimal environmental impact.

## 2. DFT Methods and Functional Advancements:

### 2.1. Local and Semi-local Functionals (LDA/GGA)

Density Functional Theory (DFT) owes much of its widespread success to the development of local and semi-local exchange–correlation functionals, particularly the Local Density Approximation (LDA) and the Generalised Gradient Approximation (GGA). These functionals form the computational backbone of most DFT calculations, offering a favourable trade-off between accuracy and computational cost. While they are often insufficient for describing systems with strong electron correlation or excited-state properties, they remain essential tools for modelling the ground-state behaviour of a vast range of materials. The Local Density Approximation simplifies the exchange–correlation energy by assuming that it depends solely on the local electron density at each point in space. Despite its simplicity, LDA performs reasonably well for systems with slowly varying densities, such as bulk metals and homogeneous electron gases. However, it commonly overbinds atoms, resulting in underestimated lattice constants and overestimated cohesive energies. This limitation led to the broader adoption of semi-local approaches such as the GGA, which incorporate density gradients to provide a more accurate representation of inhomogeneous systems (Han & Oda, 2018).

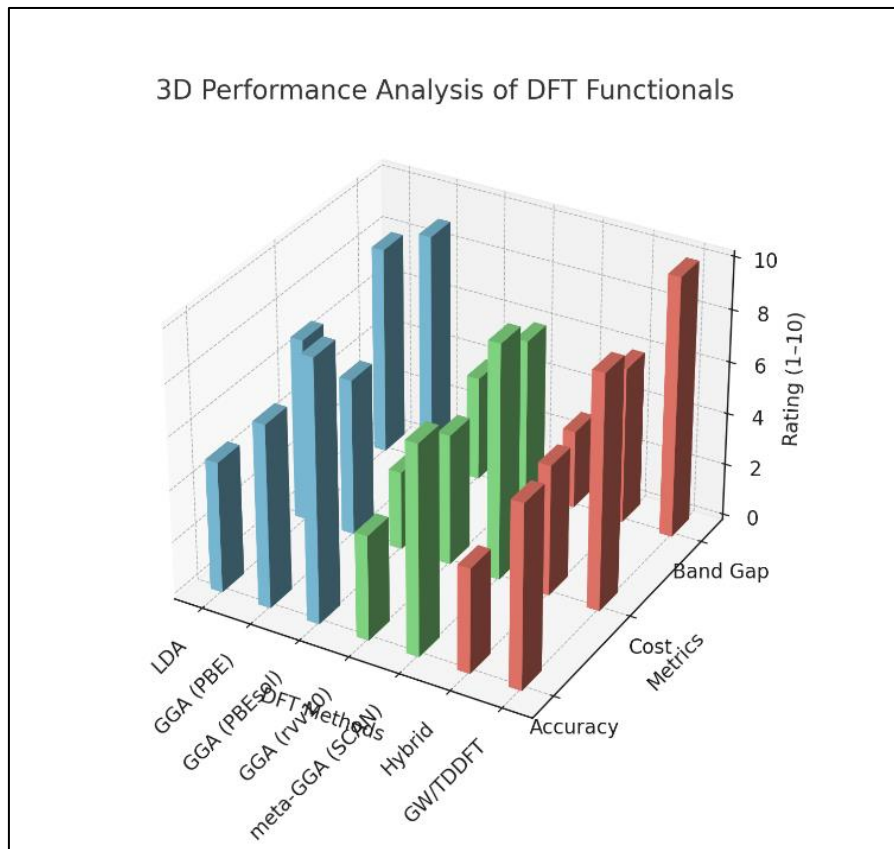
Among the GGA functionals, the Perdew–Burke–Ernzerhof (PBE) functional is one of the most widely utilised. It enhances exchange–correlation calculations and typically offers improved predictions of

structural parameters, including bond lengths, lattice constants, and formation energies (Elloh *et al.*, 2020). However, both LDA and GGA show limitations when applied to systems with more complex interactions. For instance, under high-pressure conditions in sodium, LDA was observed to underestimate atomic volumes and bulk moduli, while PBE provided more reliable structural and thermodynamic predictions (Chen *et al.*, 2025).

Furthermore, standard GGA functionals like PBE struggle to model weak van der Waals interactions accurately and often underestimate electronic band gaps in semiconductors and insulators. To mitigate these deficiencies, dispersion-corrected methods such as van der Waals-inclusive GGA (e.g., rrv10) have been introduced to better capture intermediate-range interactions (Adhikari *et al.*, 2019). Surprisingly, in certain alloy systems, PBE has even outperformed more sophisticated functionals such as SCAN (a meta-GGA functional), particularly in materials with partially filled d-orbitals. This unexpected result has been attributed to favourable error cancellation within GGA, illustrating that higher complexity does not always equate to superior accuracy (Nepal *et al.*, 2020). In electronic and optical simulations, such as those performed on PVK/C<sub>60</sub> heterostructures, both LDA and GGA have been effective in predicting band structures and density of states. Although both methods are known to

underestimate band gaps, LDA does so to a greater extent, highlighting the persistent "band gap problem" in DFT-based studies (Elloh *et al.*, 2020). An important refinement of GGA is the PBEsol functional, which was developed to improve the accuracy of structural predictions in solids by adjusting gradient corrections. In high-pressure simulations and solid-state materials modelling, PBEsol frequently shows better agreement with experimental results compared to standard PBE (Chen *et al.*, 2025).

Recent studies on complex material families such as GaM<sub>4</sub>Q<sub>8</sub> lacunar spinels have further emphasised the strengths and limitations of these functionals. While LDA was found to be inadequate in predicting structural and magnetic properties, GGA and PBEsol yielded accurate electronic structures and lattice parameters, confirming their reliability in such applications (Wang, Puggioni, & Rondinelli, 2019). Nevertheless, despite their robustness, the intrinsic simplicity of local and semi-local functionals limits their predictive power in systems with significant excited-state dynamics or long-range correlation effects. In these contexts, higher-order functionals such as meta-GGA and hybrid functionals, or alternative many-body approaches like the GW approximation and time-dependent DFT (TDDFT), are more appropriate and will be explored in subsequent sections.



**Graph: 3D performance analysis of DFT**

## 2.2. Hybrid and Meta-GGA Functionals

Hybrid and meta-GGA functionals represent significant advancements in Density Functional Theory (DFT), bridging the gap between computational efficiency and predictive accuracy for structural, electronic, and magnetic properties. These functionals are particularly valuable when conventional local or semi-local approximations such as LDA or GGA fall short, especially in systems with strong electron correlation or complex bonding environments.

Hybrid functionals incorporate a fraction of exact Hartree–Fock (HF) exchange into the exchange–correlation functional, thereby reducing the self-interaction errors common in local and semi-local approximations. Among hybrid functionals, B3LYP is extensively used for molecular systems, while HSE06—being a screened hybrid functional—has gained popularity for periodic systems due to its efficiency and enhanced accuracy in predicting band gaps (Tran *et al.*, 2021). For instance, in chalcogenide lacunar spinels such as  $\text{GaM}_4\text{Q}_8$  (where  $M = \text{Mo, V, Nb, Ta}$ ), HSE06 outperformed both GGA and meta-GGA functionals in predicting structural and electronic properties, albeit with a tendency to overestimate band gaps slightly ( $\sim 1$  eV predicted vs.  $\sim 0.2$  eV experimental) (Wang, Puggioni, & Rondinelli, 2019).

Despite their improved accuracy, hybrid functionals are computationally demanding. To address this, researchers have adopted hybrid-approximation schemes, such as performing structure relaxation using SCAN and then calculating electronic properties with HSE06, to reduce computational cost while maintaining accuracy. This approach has been particularly effective in defect calculations for halide perovskites like  $\gamma\text{-CsPbI}_3$  (Wang *et al.*, 2022). However, hybrid functionals do not always offer superior performance across all material classes. For example, in surface chemistry applications assessed through the ADS41 benchmark, HSE06 did not significantly outperform PBE or meta-GGAS in modelling molecule–surface interactions on transition metals. In some cases, MS2—a meta-GGA—provided more accurate predictions (Sharada *et al.*, 2019).

Meta-GGA functionals extend GGA's capabilities by including the kinetic energy density, enabling better distinction between different bonding environments. The SCAN (Strongly Constrained and Appropriately Normed) functional is a prominent example that delivers excellent performance in structural predictions across a wide range of materials (Rezaei, Alaei, & Oganov, 2025). In antiferromagnetic systems, SCAN and its revised form,  $r^2\text{SCAN}$ , showed exceptional agreement with experimental Néel temperatures, outperforming both GGA+U and HSE06 in predictive accuracy. An emerging meta-GGA functional, MVS (Made Very Simple), has shown promise in low-dimensional materials. In quantum spin

Hall materials like monolayer  $1\text{T}'\text{-WTe}_2$ , MVS accurately predicted a positive band gap without requiring spin–orbit coupling, Hubbard U correction, or exact exchange, surpassing GGA and performing comparably to HSE06 (Yin, Tang, & Ruzsinszky, 2024). Similarly, in wide-bandgap semiconductors such as  $4\text{H-SiC}$ , SCAN and  $r^2\text{SCAN}$  matched the accuracy of HSE06 in defect energy level prediction while being more computationally efficient (Abbas *et al.*, 2025). This efficiency makes meta-GGA functionals ideal for high-throughput screening in emerging technologies like quantum information science.

The trade-off between cost and accuracy is further exemplified in comparative studies of SCAN+U and HSE06. In one benchmark involving transition metal compounds, SCAN+U achieved mean absolute percentage errors of 1.3% in volume and 10% in band gap—comparable to HSE06 but at a fraction of the computational cost (Ao & Zhu, 2025). Innovations in meta-GGA development continue to expand their utility, particularly in low-dimensional and nanostructured materials. For example, mtask, a modified version of the TASK functional, successfully reproduced band gap values for 2D and 1D systems that were on par with HSE06 and  $G_0W_0$  calculations, making it suitable for nanoelectronic applications (Neupane *et al.*, 2021). Lastly, in complex oxide systems such as Ti- and Zr-based perovskites, meta-GGA functionals like SCAN and mbj-LDA have demonstrated high accuracy in optoelectronic predictions at significantly lower computational costs than hybrids. These results underscore the critical role of meta-GGAS in advancing photocatalytic and hydrogen production research, where material screening efficiency and accuracy are both essential (Zulficar *et al.*, 2021).

## 2.3. Time-Dependent and Beyond-DFT Methods

While Density Functional Theory (DFT) has proven highly effective for modelling ground-state properties, it often fails to accurately describe excited-state phenomena such as optical absorption spectra, quasiparticle energies, and many-body interactions. To overcome these limitations, advanced theoretical frameworks such as Time-Dependent Density Functional Theory (TDDFT) and the GW approximation—often coupled with the Bethe–Salpeter Equation (BSE)—have become essential tools in modern computational materials science (Magierski, 2019). TDDFT extends the traditional Kohn–Sham approach into the time domain, enabling simulations of excited-state dynamics and optical responses. It has become a widely used method in spectroscopy, particularly for molecules, clusters, and low-dimensional systems (Sun, Li, & Jiang, 2021). The incorporation of hybrid exchange–correlation functionals such as TD-HSE06 has further improved TDDFT's ability to capture excitonic effects, providing highly accurate optical spectra in semiconductors like  $\text{CeO}_2$  and silicon. In low-dimensional materials, TD-HSE06 has demonstrated excellent agreement with both

experimental data and GW-BSE calculations, successfully capturing interlayer and intralayer excitons in monolayer and van der Waals heterostructures (Ketola, Machacova, & Karlický, 2020).

To enhance the accuracy of TDDFT in systems with strong static correlation or fractional orbital occupations, finite-temperature TDDFT (FT-TDDFT) has been developed. This variant incorporates entropy and thermal population effects, smoothing potential energy surfaces and improving simulations of  $\pi$ -conjugated systems (Yoshikawa, Doi, & Nakai, 2020). Meanwhile, the use of long-range corrected (LRC) exchange-correlation kernels in TDDFT has enabled better exciton binding predictions. However, these kernels may violate the zero-force theorem in real-time simulations, requiring careful numerical stabilisation to prevent instability at high exciton energies (Williams & Ullrich, 2025). Ongoing research also explores reducing the computational cost of orbital-dependent TDDFT methods. Local-scaling approximations to the time-dependent optimised effective potential (TDOEP) offer a promising route to simulate time-dependent electron dynamics more efficiently while preserving essential exchange effects (Guarezzi & Vieira, 2020). Despite these improvements, TDDFT often underestimates exciton binding energies and fails to fully capture quasiparticle properties, especially in materials with strong electron-hole interactions.

For more accurate excited-state properties, the GW approximation provides a powerful alternative. By correcting the DFT-derived eigenvalues through self-energy calculations, GW significantly improves the accuracy of band gaps and quasiparticle energies (Pham *et al.*, 2021). When combined with the Bethe–Salpeter Equation, the GW-BSE framework accurately models excitonic effects by accounting for electron–hole interactions, making it superior for optical and excitonic simulations. In organic fluorophores operating in the NIR-II window, GW-BSE has achieved near-experimental precision, outperforming TDDFT in spectral resolution and binding energy estimation (Pham *et al.*, 2021). The importance of GW-BSE is further highlighted in studies on photocatalytic materials like  $\text{Bi}_2\text{WO}_6$ , where DFT alone failed to replicate experimental optical absorption data. In contrast, GW-BSE successfully revealed bound exciton states consistent with observations (Ahmad *et al.*, 2021). Even in cases where complete GW calculations are not feasible, TDDFT equipped with advanced exchange-correlation kernels such as the Bootstrap kernel can approximate excitonic features. This approach has proven helpful in two-dimensional materials like  $\text{MoS}_2$  and h-BN, accurately distinguishing between interlayer and intralayer excitons in bilayer systems (Suzuki & Watanabe, 2019). For larger and more complex systems, quasiparticle self-consistent GW (qsGW) eliminates dependence on the initial DFT input and yields highly accurate electronic excitations. When combined with

BSE, qsGW-BSE has demonstrated remarkable success in reproducing experimental spectra in large chromophore assemblies like chlorophyll dimers, involving systems with more than 2000 electrons (Förster & Visscher, 2022). Similarly, in low-dimensional structures such as selenium and tellurium nanowires, GW-BSE has confirmed strong confinement-induced exciton binding energies exceeding two eV, emphasising the power of beyond-DFT methods for nanoscale optoelectronic design (Andharia, 2018).

### 3. DFT in Solar Cell Material Modelling:

#### 3.1. Band Structure Engineering of Semiconductors

Density Functional Theory (DFT) plays a pivotal role in the band structure engineering of semiconductors, enabling precise control over electronic properties that are crucial for photovoltaic applications. Among these, band gap tuning, defect state management, and the transition between direct and indirect band gaps are particularly important as they directly impact light absorption efficiency, carrier lifetime, and power conversion efficiency in solar cells. One of the most effective strategies for band gap engineering is through external modulation, such as pressure, doping, or alloying. For instance, in the lead-free double perovskite  $\text{Cs}_2\text{AgBiCl}_6$ , DFT simulations demonstrated that applying hydrostatic pressure can drive a transition from an indirect to a direct band gap, reducing the band gap energy from 2.6 eV to approximately 1.6 eV, thereby significantly enhancing visible light absorption (Islam & Podder, 2022). Similarly, in  $\text{Cs}_2\text{AgBiBr}_6$ , antisite defect engineering transforms its electronic structure from an indirect to a direct band gap, lowering the gap from 2.04 eV to 1.59 eV. This structural disorder improves optical absorption and carrier generation, making the material more suitable as a solar absorber (Hadi, Islam, & Podder, 2022).

Defect manipulation using DFT has also proven valuable in traditional materials such as  $\text{Cu}_2\text{O}$ . The introduction of oxygen vacancies alters the band structure and induces a shift from direct to indirect transitions. Nitrogen doping, on the other hand, stabilises a direct band gap around 1.09 eV while suppressing mid-gap states that typically cause recombination, thus improving visible light harvesting (Idowu *et al.*, 2024). In Gap nanostructures, surface engineering enables a transformation from an indirect to a direct band gap without modifying the bulk composition. This structural control results in a photoluminescence enhancement of over 400%, indicating the potential of such modifications for advanced optoelectronic devices (Califano, Lu, & Zhou, 2021). Electric field tuning provides another reversible pathway for band gap control. In monolayer  $\text{InSe}$ , a perpendicular electric field has been shown to induce a reversible shift between indirect and direct band gaps, and even narrow the gap toward metallicity. This level of tunability allows for dynamic modulation of optoelectronic properties in real-time applications (Xiao *et al.*, 2019). Layer-dependent band structure changes are

also a defining characteristic of two-dimensional transition metal dichalcogenides (TMDS) like MoS<sub>2</sub> and WS<sub>2</sub>. DFT studies confirm that these materials exhibit a direct band gap at the K-point in monolayer form, which shifts to an indirect gap as additional layers are introduced. This transition is highly sensitive to interlayer spacing and strain, making them versatile platforms for band engineering (Ortenzi, Pietronero, & Cappelluti, 2018). In bilayer heterostructures such as WSe<sub>2</sub>/WS<sub>2</sub> and MoSe<sub>2</sub>/MoS<sub>2</sub>, DFT calculations show that stacking order and strain alignment can shift the electronic structure from indirect to direct band gap, enhancing exciton generation under solar irradiation (Dange, Yogi, & Shukla, 2025). Experimental-DFT studies have validated these predictions. For example, BaLaCuS<sub>3</sub> was found to possess a direct band gap of ~2.0 eV, making it a promising material for underwater photovoltaics (Oreshonkov *et al.*, 2021). In few-layer InSe, combined photoemission and photoluminescence experiments with DFT modeling revealed a transition from a direct to indirect band gap as thickness decreased from six to two layers, attributed to quantum confinement and orbital hybridization effects (Hamer *et al.*, 2019).

Advancements in machine learning have further enhanced the predictive capabilities of DFT-based band gap engineering. A 2024 study integrated regression and classification models trained on DFT data to identify 30 new photovoltaic materials capable of shifting from indirect to direct band gaps upon alloying, with each prediction validated through DFT calculations (Dinic, Neporozhnyi, & Voznyy, 2024). Furthermore, HSE06-based defect studies in monolayer MoS<sub>2</sub> revealed that chalcogen vacancies introduce mid-gap states and convert the semiconductor from direct to indirect, negatively impacting light absorption and charge separation (Pawar & Sangolkar, 2021). These examples collectively demonstrate the power of DFT in predicting and tuning the electronic properties of semiconductors, guiding the rational design of next-generation solar energy materials through a combination of theoretical insight and computational efficiency.

### 3.2. Charge Transport and Recombination Mechanisms

Efficient charge transport and minimized carrier recombination are essential requirements for achieving high power conversion efficiency (PCE) in photovoltaic devices. Density Functional Theory (DFT) provides a valuable theoretical framework to analyze and optimize these properties by enabling atomistic insights into effective carrier mass, density of states, carrier mobility, and recombination centers. In the context of perovskite solar cells, trap states at grain boundaries and interfacial regions significantly hinder charge transport. DFT studies have shown that incorporating thiocyanate-passivated Dion–Jacobson phase 2D perovskites effectively reduces trap density and enhances charge mobility, resulting in a notable improvement in PCE

from 10.3% to 15.08% (Yukta *et al.*, 2022). A key parameter influencing transport is the effective mass of charge carriers. In Fe/S-doped TiO<sub>2</sub> electron transport layers (ETLs), DFT simulations revealed that doping reduces the effective mass of electrons, thereby increasing their mobility and lowering recombination rates. These enhancements contributed to a PCE gain of over 1.4% compared to undoped systems (Dharmale *et al.*, 2024). Beyond dopant effects, intrinsic lattice interactions also play a crucial role. Large polaron formation in halide perovskites—caused by strong electron–phonon coupling—has been identified via DFT as a mechanism that enhances mobility by shielding carriers from scattering. This phenomenon helps explain the remarkable defect tolerance of perovskite materials and supports their continued use in high-efficiency devices (Zhang & Park, 2023).

DFT-guided studies in mixed Sn–Pb halide perovskites revealed that carrier mobility is strongly influenced by longitudinal optical (LO) phonon scattering. A critical finding was that Pb content exceeding 50% leads to an increase in carrier effective mass and a reduction in mobility, due to an electronic crossover that increases the density of scattering centers (Teeratchanan *et al.*, 2024).

Interface engineering also plays a decisive role in modulating charge transport. Incorporating brominated graphene oxide (Br-GO) at the interface in CsPbBr<sub>3</sub>-based devices improved hole mobility and reduced trap densities, as shown by DFT-based electronic structure analyses. These modifications resulted in better band alignment, minimized non-radiative recombination, and increased PCE from 6.28% to 10.1% (Sun *et al.*, 2021). Similar improvements have been achieved using CuO<sub>x</sub> quantum dot-based interfacial layers in inverted perovskite solar cells. DFT simulations demonstrated that CuO<sub>x</sub> facilitates efficient hole transport and suppresses trap states, resulting in a PCE enhancement from 17.4% to 19.91% (Ma *et al.*, 2021). Emerging techniques such as the carrier-resolved photo-Hall effect have combined DFT modeling with experimental data to non-invasively extract key transport parameters—mobility, trap density, and recombination lifetime—in halide perovskites. This method has revealed detailed insights into the role of trap-limited transport in practical devices (Gunawan *et al.*, 2024).

In organic photovoltaics, doping-induced trap filling has emerged as an effective strategy for suppressing non-radiative recombination and enhancing carrier lifetimes. Transient absorption spectroscopy, supported by DFT models, has shown that doping improves transport properties and efficiency in systems like PCE10/PC<sub>71</sub>BM (Hou *et al.*, 2018). Furthermore, time-resolved experimental approaches have been employed to assess carrier mobility under operational conditions. DFT simulations have helped clarify how low-energy trap occupation affects mobility on

microsecond timescales, providing a nuanced understanding of both field- and material-dependent transport behavior (Jasiūnas *et al.*, 2021).

Finally, studies on interface-modified  $\text{TiO}_x$  electron transport layers in planar perovskite solar cells underscore the importance of interfacial engineering guided by DFT. Introducing fullerene-based interfacial modifiers with inherently higher mobility and reduced

defect density led to superior charge extraction, enhanced current density, and significant PCE improvements (Shahiduzzaman *et al.*, 2018). Together, these findings underscore the indispensable role of DFT in deciphering and enhancing charge transport and recombination dynamics, informing strategies to engineer more efficient, defect-tolerant, and stable photovoltaic devices.

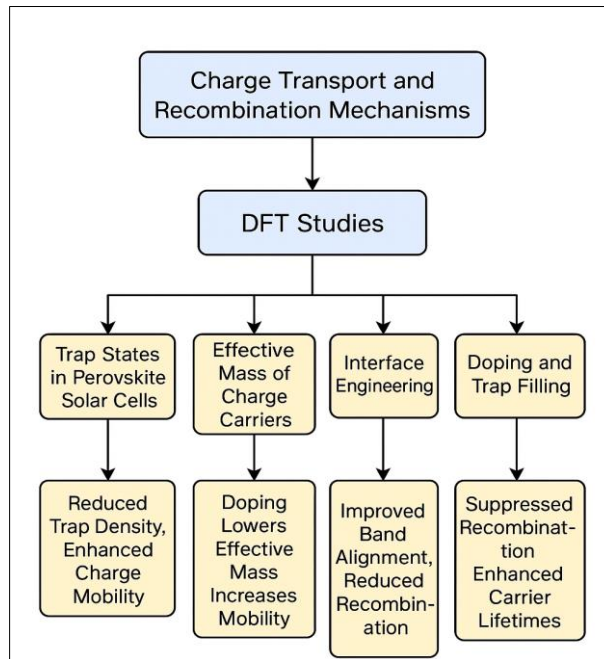


**Figure: DFT-Guided Insights into Charge Transport and Recombination Mechanisms in Photovoltaic Devices**

### 3.3. Interface and Heterojunction Simulations

The accurate simulation of interfaces and heterojunctions plays a pivotal role in the rational design of high-efficiency solar cells. Density Functional Theory (DFT) provides atomistic-level insights into band alignment, interfacial bonding, and the formation of surface states, all of which critically influence charge transfer, separation, and recombination dynamics. In perovskite-based photovoltaics, DFT studies have revealed significant effects of interfacial interactions. For example, simulations involving  $\text{MAPbI}_3$  interfaced with  $\text{C}_{60}$  and  $\text{C}_{70}$  fullerenes demonstrated that spin-orbit coupling reshapes interfacial energy levels, influencing electron transfer rates. Notably, the  $\text{MAPbI}_3/\text{C}_{70}$  interface exhibited superior interfacial dynamics compared to  $\text{MAPbI}_3/\text{C}_{60}$ , resulting in more efficient carrier extraction (Yang *et al.*, 2021). Hybrid DFT modelling of  $\text{MAPbI}_3/\text{TiO}_2$  heterojunctions functionalised with 4-chlorobenzoic acid (CBA) revealed almost complete electron transfer from perovskite to  $\text{TiO}_2$ . This effect was attributed to enhanced interfacial bonding and favourable band alignment, improving device performance (Su *et al.*, 2020).

For  $\text{Ga}_2\text{O}_3/\text{Ge}$  heterostructures, DFT-calculated valence and conduction band offsets of 3.26 eV and 0.87 eV, respectively, identified the system as promising for high-voltage optoelectronic applications (Yang *et al.*, 2024). Similarly, in CdTe-based solar cells, simulations of  $\text{Mg}_x\text{Zn}_{1-x}\text{O}/\text{CdTe}$  interfaces showed that interfacial strain and crystallographic orientation significantly alter the conduction band alignment. These factors strongly influence back contact behaviour and recombination losses, guiding interfacial engineering (Thiyagarajan & Sampath, 2019). Emerging two-dimensional/three-dimensional (2D/3D) heterostructures also benefit from interface engineering. In  $\text{CHA}_2\text{PbI}_4/3\text{D}$  perovskite junctions, spontaneous valence band alignment enhanced hole extraction, boosting power conversion efficiency from 20.4% to 23.9% (Jeong *et al.*, 2021). Beyond traditional semiconductors, phosphorene nanoribbon heterostructures functionalised with hydroxyl and OCN groups were shown via DFT and nonadiabatic molecular dynamics to form direct Z-scheme junctions. These structures feature strong built-in electric fields that promote ultrafast charge separation (Gao *et al.*, 2021). In  $\text{ZnO}/\text{graphene}$  van der Waals heterojunctions, plasma-induced oxygen vacancies created mid-gap states. They shifted the Fermi level by 0.73 eV, optimising charge

separation and enhancing UV-light-driven solar energy conversion (Gong *et al.*, 2022).

Advancements in data-driven materials modelling have also been applied. Machine-learning-assisted DFT simulations of Cds/CdTe interfaces showed that interfacial disorder significantly impacts valence band offset ( $\sim 0.55$  eV), providing critical insights for passivation and band engineering strategies (Tang *et al.*, 2020). Finally, for MAPbI<sub>3</sub> interfaced with fluorinated Zn-phthalocyanines (FnZnPc), DFT studies indicated that increased fluorination tunes the ionisation potential without compromising hole mobility, thereby validating their application in interface layers for improved charge transport (Oleiki, Javaid, & Lee, 2022).

## 4. Perovskite Solar Cells: Insights from DFT

### 4.1. Structural Optimisation and Stability

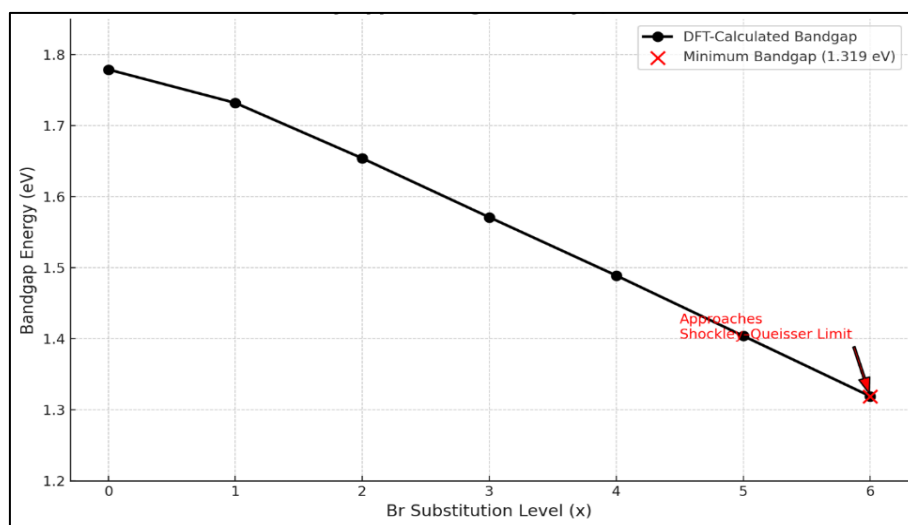
Stability is one of the critical challenges facing perovskite solar cells, particularly hybrid organic–inorganic perovskites with the general formula ABX<sub>3</sub>. Density Functional Theory (DFT) has played a central role in understanding the structural dynamics of these materials, including lattice distortions, phase transitions, and ion migration pathways. DFT-based phonon calculations of CsPbI<sub>3</sub> revealed strong anharmonic instabilities linked to double-well potentials at the Brillouin zone centre. These instabilities contribute to spontaneous phase transitions to the non-photoactive yellow  $\delta$ -phase, underlining the importance of vibrational entropy and symmetry breaking in maintaining phase stability (Marronnier, 2018). A high-throughput DFT screening of over 14,000 ABX<sub>3</sub>-type materials identified key stability descriptors, such as formation energy, energy above hull, and Goldschmidt tolerance factors.

This approach led to more than 600 stable perovskite oxides and oxynitrides suitable for photovoltaic applications (Priyanga *et al.*, 2024). DFT simulations also showed that incorporating small alkali

cations like Rb<sup>+</sup> and K<sup>+</sup> at interstitial sites enhances phase stability by increasing ion migration barriers. Experimental validation via temperature-dependent conductivity and hysteresis measurements confirmed the stabilisation of the black phase and reduced ionic mobility (Tao *et al.*, 2018). Moreover, halide vacancies were identified as key contributors to ion migration under electric fields, light, and temperature gradients. DFT simulations of CsPbX<sub>3</sub> (X = Cl, Br, I) quantified migration barriers and mapped potential energy surfaces, providing insights for defect engineering to suppress degradation (Woo *et al.*, 2022).

### 4.2. Electronic and Optical Properties

DFT methods have significantly advanced the understanding of electronic structures in perovskite solar materials, including bandgap engineering, defect tolerance, and light absorption characteristics. Comprehensive DFT studies on ABX<sub>3</sub> halide perovskites have demonstrated their tunable band gaps, extending from the ultraviolet to the near-infrared region depending on A-site and X-site substitutions. This broad tunability facilitates optimised absorption across the solar spectrum (Murad *et al.*, 2021). In Cs<sub>3</sub>GaI<sub>6-x</sub>Br<sub>x</sub> (0  $\leq$  x  $\leq$  6), band gaps were successfully tuned from 1.779 eV to 1.319 eV, approaching the Shockley–Queisser efficiency limit. The materials also exhibited high absorption coefficients ( $>10^4$  cm<sup>-1</sup>), indicating excellent photovoltaic potential (Ahmed *et al.*, 2022). DFT predictions on inorganic halide perovskites such as CsRbTeX<sub>6</sub> (X = I, Br, Cl) revealed indirect band gaps between 1.51 and 2.81 eV, with strong optical absorption and mechanical flexibility, making them ideal for thin-film devices (Harbi, Aziz, & Moutaabbid, 2023). Furthermore, machine learning models trained on DFT-generated data have been used to rapidly predict the density of states and absorption characteristics for over 80 ABX<sub>3</sub> perovskite compositions, significantly accelerating material discovery (Alhashmi, Kanoun, & Goumri-Said, 2023).



**Graph: "DFT-Predicted Bandgap Tunability in Cs<sub>3</sub>GaI<sub>6-x</sub>Br<sub>x</sub> (0  $\leq$  x  $\leq$  6): Approaching Shockley–Queisser Limit"**

### 4.3. DFT Modelling of Toxicity and Degradation

Environmental sustainability is a significant concern in perovskite technology due to the presence of lead. DFT offers deep insights into degradation mechanisms, leaching behaviour, and design strategies for lead-free alternatives. DFT-calculated formation energies showed that  $\text{Pb}^{2+}$  ions tend to leach under humid conditions or external electric bias due to low-energy diffusion channels, contributing to surface decomposition and device instability (Woo *et al.*, 2022). Efforts to replace lead with less toxic elements such as Ga, Ge, and Sn have been explored through DFT. For example, in  $\text{KGeI}_{3-x}\text{Br}_x$  systems, DFT predicted tunable bandgaps (0.611 to 1.126 eV) and high thermodynamic stability, supporting their use as potential lead-free perovskites (Hamideddine *et al.*, 2021). Double perovskites like  $\text{Cs}_2\text{PdBr}_{6-x}\text{I}_x$  have shown remarkable optical properties and tunable band gaps (0.77–1.73 eV). DFT calculations confirmed their thermodynamic stability and non-toxic composition, highlighting them as promising materials for eco-friendly devices (Li *et al.*, 2023). DFT simulations also emphasised alkali interstitial doping (e.g.,  $\text{Rb}^+$ ,  $\text{K}^+$ ), which increases ion migration barriers, reduces hysteresis, and extends device lifetimes by suppressing ion diffusion and improving stability (Cao *et al.*, 2018).

## 5. DFT in Silicon and Thin-Film Photovoltaics

### 5.1. Crystalline and Amorphous Silicon

Crystalline silicon (c-Si) remains the dominant material in commercial photovoltaic devices due to its natural abundance, non-toxicity, and high thermal and chemical stability. However, developing next-generation solar technologies demands a deeper understanding of silicon-based systems at the atomic level, which is effectively addressed by Density Functional Theory (DFT). DFT has emerged as a critical tool for modelling electronic structure, defect formation, and interface behaviour in both crystalline and amorphous silicon systems. One of the key insights from DFT simulations relates to the impact of deposition processes on crystalline silicon during the formation of transparent conductive oxide (TCO) contacts. For example, indium tin oxide (ITO) deposition via reactive plasma introduces recombination-active defects in c-Si, manifesting as photoluminescence peaks at 0.767 eV and 0.614 eV. These energy levels are associated with irradiation-induced defects that degrade carrier lifetime and overall solar cell performance (Kojima *et al.*, 2023).

In parallel, DFT has provided valuable guidance for improving heterojunction designs, particularly through analysis of amorphous silicon (a-Si: H) layers used for surface passivation. Simulations have shown that increasing the defect density, especially dangling bonds, in p-type a-Si: H negatively impacts solar cell efficiency by facilitating recombination and reducing the open-circuit voltage. These effects stem primarily from unfavourable charge redistribution at the a-Si: H/c-Si interface (Balent *et al.*, 2021). To address

such limitations, interface engineering strategies have been developed. One approach involves inserting an ultrathin intrinsic a-Si: H interlayer between the doped a-Si: H and crystalline silicon, which has proven effective in reducing interface defect density and enhancing field-assisted carrier separation. DFT-supported electrical modelling confirms that surface passivation quality is inversely proportional to defect density, with open-circuit voltage dropping significantly when defect concentrations exceed  $10^{11} \text{ cm}^{-2}$  (Rached & Rahal, 2020).

Advancements in silicon heterojunction (SHJ) solar cells have also been realised through carefully optimising doped a-Si: H(p) emitter layers. Specifically, adjusting the doping level and minimising layer thickness has been shown to strengthen the electric field at the heterointerface, thereby improving quantum efficiency and boosting open-circuit voltages from 0.60 V to as high as 0.705 V in optimised structures (Kanneboina, Madaka, & Agarwal, 2021). Another innovative technique, catalytic impurity doping (Cat-doping), provides a low-temperature method to form boron-doped a-Si: H emitters. DFT analysis has demonstrated that Cat-doping improves tunnelling conduction across the ITO/a-Si: H interface, enabling the development of efficient SHJ solar cells with open-circuit voltages exceeding 0.6 V (Akiyama & Ohdaira, 2018).

For SHJ designs that omit TCO layers altogether, DFT simulations paired with experimental validation have revealed that direct aluminium (Al) interfacial with p-type a-Si: H, followed by annealing, forms an aluminium silicide contact. This configuration supports efficient tunnelling recombination and significantly reduces specific contact resistivity, improving fill factors up to 77.5% (Wagner *et al.*, 2021). Meanwhile, the TCO layers themselves have been extensively optimised using DFT insights. For instance, reducing the oxygen concentration in ITO during the deposition process has enhanced carrier concentration and reduced resistivity, thereby improving electrical contact quality. A bilayer TCO structure—comprising a low-oxygen ITO interlayer and a high-oxygen bulk layer—has been proposed as an optimal balance between optical transparency and electrical performance (Luderer *et al.*, 2021).

Finally, numerical simulations using AFORS-HET software, informed by DFT data, have confirmed that precise control over interface defect states, doping profiles, and oxide work functions can push power conversion efficiencies to over 23.6%. These computational findings offer a robust theoretical foundation for developing and refining high-performance heterojunction with intrinsic thin layer (HIT) solar cell architectures (Satriani *et al.*, 2023).

## 5.2. CIGS and CZTS Materials

The advancement of high-efficiency and earth-abundant thin-film photovoltaic materials has positioned copper indium gallium selenide (CIGS) and copper zinc tin sulfide (CZTS) as leading candidates in next-generation solar cell research. Density Functional Theory (DFT) has played a central role in analysing these quaternary chalcogenide semiconductors' electronic, structural, and defect-related properties, thereby guiding synthesis techniques, doping methods, and defect suppression strategies. A comprehensive high-throughput DFT screening of 540 ternary and quaternary chalcogenides ( $ABX_2$  and  $A_2BCX_4$ ) identified 45 candidates with a spectroscopic limited maximum efficiency (SLME) exceeding 30%. Among them, several CIGS and CZTS analogs were highlighted as stable, direct bandgap absorbers with high optical absorption and favorable defect profiles, positioning them as viable absorber materials for scalable thin-film technologies (Rahman & Mannodi-Kanakkithodi, 2025).

Further DFT investigations comparing functional types in CZTS and its germanium-substituted variant CZGS revealed that hybrid functionals like HSE06 and meta-GGA, such as SCAN, significantly outperform standard PBE in accurately predicting defect formation energies and band structures. It was shown that antisite defects, especially Cu substituting Sn ( $Cu_{Sn}$ ), are susceptible to the choice of functional and are primarily responsible for the open-circuit voltage losses observed in actual devices (Wexler, Gautam, & Carter, 2020). First-principles studies of point defects in CZTS confirmed that Cu–Zn disorder introduces deep-level states within the bandgap, which act as recombination centres. As a result, DFT-guided synthesis has shifted toward conditions and compositional strategies—like partial Ge substitution and alkali metal doping—that help suppress such antisite formations (Mangelis *et al.*, 2019). The optoelectronic characteristics of CZTS can also be optimised by adjusting cation composition. For instance, replacing Cu with Ag in the A site of  $A_2ZnSnS_4$  to form  $Ag_2ZnSnS_4$  has been found to improve cation ordering and increase the bandgap, which is advantageous for tandem solar cell integration (Delgado, Delgado-Niño, & Quintero, 2021). Moreover, alloying and doping provide powerful means to tailor band structure and optical properties. DFT studies on  $Ag_2MgSn(S/Se)_4$  systems revealed that both kesterite and stannite phases exhibit direct band gaps between 1.2 and 1.6 eV and possess high absorption coefficients in the visible range, reinforcing their suitability for absorber layers in solar devices (Srivastava *et al.*, 2020).

CIGS absorbers have also been the subject of extensive DFT-based doping studies. For example, a comparative analysis of post-deposition treatments with light (Li) and heavy (Cs) alkali metals in  $CuGaSe_2$  and CIGS structures demonstrated that Cs significantly alters surface morphology. At the same time, Li provides more

effective defect passivation. These behaviours were attributed to differences in dopant formation energies and diffusion barriers derived from total energy DFT calculations (Ishizuka *et al.*, 2020). In addition, newer quaternary chalcogenides like  $In_4Pb_{5.5}Sb_5S_{19}$  have drawn attention for their ideal bandgap (~1.42 eV), ambient chemical stability, and low thermal conductivity. DFT simulations coupled with experimental X-ray and calorimetric analysis validated their thermodynamic suitability for photovoltaic applications (Li *et al.*, 2020). In chalcopyrite-based systems, alloying  $Cu_{1-x}Ag_xGaTe_2$  with ZnTe has been modelled using hybrid DFT, revealing a non-parabolic band structure and mid-gap impurity states that optimise both Seebeck coefficient and charge carrier concentrations. Cu vacancies and ZnTe incorporation improve electrical conductivity while suppressing thermal conductivity, leading to materials with promising dual photovoltaic and thermoelectric applications (Xie *et al.*, 2022). Even more advanced chalcopyrites like  $CsZrCuSe_3$  have demonstrated highly tunable direct bandgaps (~1.32 eV), intense absorption in the violet-blue region, and notable thermoelectric properties. HSE06-based DFT modelling combined with Boltzmann transport calculations confirmed this material's potential for multifunctional energy devices (Goumri-Said *et al.*, 2024).

## 5.3. Interface Modeling with Transparent Conducting Oxides (TCOs)

Transparent conducting oxides (TCOs) such as indium tin oxide (ITO), fluorine-doped tin oxide (FTO), and aluminium-doped zinc oxide (AZO) play a crucial dual role in thin-film solar cells as both light-transmitting windows and charge-conducting layers. These materials are widely used in silicon, CIGS, CZTS, and CdTe-based devices, yet their interfaces often introduce performance-limiting factors such as interfacial recombination and parasitic absorption. Density Functional Theory (DFT) modelling has become an indispensable tool for exploring band alignment, defect formation, and chemical interactions at the interfaces between TCOs and absorber materials. In bifacial and tandem CIGS devices, the thickness of the ITO back contact significantly alters the band structure at the interface. A recent study found that increasing ITO thickness from 80 to 320 nm led to a 0.029 eV widening of the optical bandgap due to the Burstein–Moss shift, which corresponded to a 0.023 V increase in open-circuit voltage by reducing the Schottky barrier height at the CIGS/ITO interface (Ali *et al.*, 2024).

TCO stacks combining ITO with Al-doped ZnO (AZO) for silicon solar cells have shown high passivation quality in simulations and experiments. Placing a highly doped AZO layer beneath ITO effectively suppresses hole concentrations at the surface and enhances the minority carrier lifetime. This structure has yielded an implied open-circuit voltage of ~700 mV and carrier lifetimes as high as 2.0 ms (Yue *et al.*, 2023).

Additionally, atomic layer deposition of ZnO-based TCOS, capped with  $\text{Al}_2\text{O}_3$ , has been shown to prevent hydrogen effusion during thermal annealing. This TCO/ $\text{Al}_2\text{O}_3$  stack significantly lowers surface recombination velocities on n-type silicon to just 4.8 cm/s, offering promising pathways for improving monolithic silicon heterojunction solar cells (van de Loo *et al.*, 2019). In organic solar cells, AZO-based TCOS offer high transmittance in the UV region below 380 nm and mechanical flexibility suitable for flexible device applications. When paired with ZnO as the electron transport layer and Spiro-OMeTAD as the hole transport layer, these AZO-based interfaces exhibit reduced recombination losses and achieve power conversion efficiencies exceeding 10.2% (Gogoi & Das, 2023). In the context of ultrathin CIGSe devices deposited on ITO, a post-deposition treatment using sodium fluoride (NaF) transitions the back contact from a Schottky to an Ohmic interface. This transition enhances back-contact conductivity, reduces recombination losses, and improves device efficiency from 8.7% to 12.9% for films thinner than 500 nm (Li *et al.*, 2021).

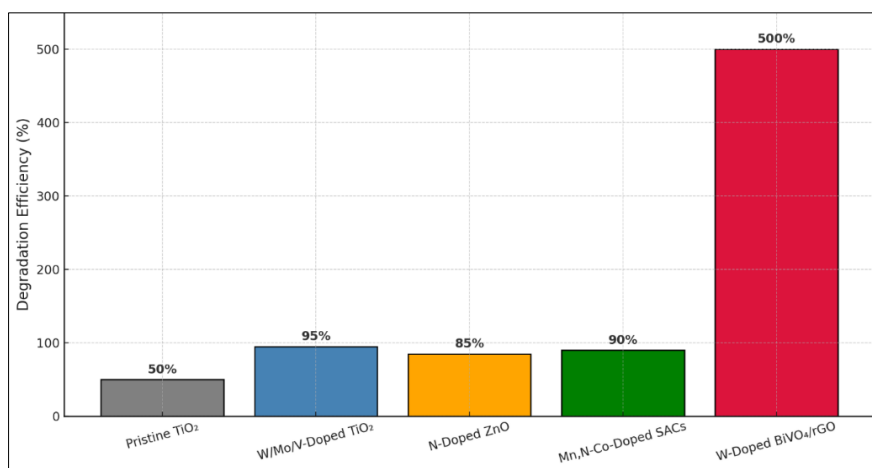
CdTe solar cells also benefit from 464ptimizin TCO interfaces. Introducing a nanocomposite ZnS: Cu interlayer between the absorber and the ITO back contact improves bifacial illumination performance and decreases rear-side recombination. This structure maintains high transparency (>70%) and improves long-term contact stability under operational conditions (Subedi *et al.*, 2018). In a simulation-based study of ZnO-Cds-Sns-Nio-Au solar cells, interface state densities at the ZnO/Sns and Nio/Sns junctions were found to be critical performance determinants. SCAPS modelling supported by DFT parameters suggested that 464ptimizing the TCO work function and reducing interfacial trap density could push the power conversion efficiency as high as 26.9% (Umar *et al.*, 2022). A final comparative study examined  $\text{Cu}_2\text{ZnSnSe}_4$  (CZTSe) devices grown on different TCO substrates, namely ZnO: Al and FTO, in contrast to the traditional molybdenum (Mo) back contact. It was revealed that TCOS, while

beneficial in some respects, act as barriers to sodium diffusion and alter grain morphology at the interface. Devices grown on Mo reached 8% efficiency, whereas those on FTO performed poorly (2.3%) due to the formation of interfacial ZnO and elevated recombination rates (Temgoua *et al.*, 2019).

## 6. Photocatalytic Water Treatment Materials:

### 6.1. $\text{TiO}_2$ and Doped Oxides for Photodegradation

Titanium dioxide ( $\text{TiO}_2$ ) remains among the most extensively studied photocatalysts due to its abundance, chemical stability, and strong oxidative capabilities. The anatase phase, in particular, offers superior photocatalytic activity compared to rutile and brookite. However, pristine  $\text{TiO}_2$  is limited by rapid recombination of photogenerated charge carriers and insufficient absorption in the visible spectrum. Density Functional Theory (DFT)-guided approaches have enabled significant doping and defect engineering advances to overcome these limitations. Transition metal doping using elements such as tungsten, molybdenum, and vanadium has been shown via DFT calculations to narrow  $\text{TiO}_2$ 's bandgap and stabilise the anatase structure while promoting charge separation. These modifications enhanced methylene blue degradation by more than 95% under visible light exposure (Manojkumar *et al.*, 2020). Similarly, nitrogen-doped ZnO photocatalysts synthesised via green methods demonstrated improved crystallinity and the creation of intermediate bandgap states, increasing visible-light-driven degradation of methylene blue (Humairah *et al.*, 2025). In a separate study, biochar-supported Mn and N co-doped single-atom catalysts were found effective in degrading sulfanilamide, with DFT results highlighting the synergistic role of d- and p-orbital electrons in enhancing redox capacity while retaining low toxicity (Dong *et al.*, 2023). The role of oxygen vacancies (OVS) has also gained attention, particularly in W-doped  $\text{BiVO}_4/\text{rGO}$  composites, where OVS introduce mid-gap states that expand light absorption and improve charge separation. As a result, pollutant degradation efficiency increased more than tenfold (Zhao *et al.*, 2021).



**Graph: Photocatalytic Degradation Efficiency of  $\text{TiO}_2$ -Based Materials (Derived from DFT-Guided Enhancement)**

## 6.2. Metal-Organic Frameworks (MOFS)

Metal-organic frameworks (MOFS), with their high surface areas and tunable porosity, offer a modular platform for photocatalysis. DFT-guided design strategies optimise their band structures and catalytic centers for environmental applications. Porphyrin-based MOFs such as PCN-223, PCN-224, and MOF-525 have been evaluated under saline wastewater conditions, with DFT simulations confirming enhanced bisphenol A (BPA) adsorption and electron transfer capabilities in the presence of competing ions (Wang *et al.*, 2022). Moreover, Ti-doped Zr-UiO-66-NH<sub>2</sub> achieved 99.8% removal of tetracycline and Cr(VI) from water, driven by improved charge transfer from Zr to Ti. It reduced recombination rates, as validated by DFT modelling (Gao *et al.*, 2023). A phosphorus-doped Co<sub>3</sub>O<sub>4</sub> catalyst derived from ZIF-67 displayed a 39-fold improvement in hydrogen evolution over the pristine MOF, with DFT analysis showing that P-doping fine-tuned surface electron delocalisation and lowered activation energy for H<sub>2</sub> production at Co-P-O sites (Zhang, Jin, & Tsubaki, 2021). The photocatalytic potential of MOFS has been further advanced by hybridising them with semiconductors, which enhances charge transfer and reduces recombination, as demonstrated in recent DFT-supported studies (Jabbar *et al.*, 2024).

## 6.3. Carbon-Based Nanomaterials in Wastewater Applications

Carbon-based nanomaterials, especially graphene oxide (GO) and its derivatives, are increasingly employed in wastewater treatment due to their high surface area, adsorption properties, and facilitation of charge transport. In composite systems involving GO, Bi<sub>2</sub>WO<sub>6</sub>, BiPO<sub>4</sub>, and Ag nanoparticles, an optimal GO content of 2.4 wt% significantly enhanced the photodegradation of amoxicillin and methylene blue. DFT-assisted mechanistic studies elucidated degradation pathways and the role of reactive radicals in pollutant breakdown and bacterial inactivation (Ma *et al.*, 2023). A Mn-NGO single-atom catalyst achieved high sulfanilamide removal efficiencies. DFT confirmed the enhanced electron delocalisation between Mn and N atoms and intense interactions with polar groups on the pollutant molecule (Lyu *et al.*, 2022). Similarly, ZNC/rGO nanocomposites synthesised from ZIF-8 achieved 98.9% methylene blue degradation under sunlight, supported by DFT and electrochemical analyses showing improved charge separation and reduced recombination due to synergistic conductivity between doped ZnO and rGO (Kaid *et al.*, 2022). In another advanced system, GO/Ni:FeOOH/silicon nanowire photocatalysts facilitated a 5.7-fold increase in hydroxyl radical production compared to H<sub>2</sub>O<sub>2</sub>-only systems. The built-in electric field between components enabled directional charge transport, significantly enhancing the degradation of diverse pollutants (Ning *et al.*, 2023).

## 7. Modeling Water Splitting and Hydrogen Evolution:

### 7.1. Band Edge Alignment for HER and OER

Efficient photocatalytic water splitting requires precise alignment of a semiconductor's band edges with the redox potentials of water. Specifically, the conduction band minimum (CBM) must lie above the hydrogen evolution reaction (HER) potential (0 V vs. NHE). In comparison, the valence band maximum (VBM) should lie below the oxygen evolution reaction (OER) potential (+1.23 V vs. NHE) to facilitate spontaneous water splitting under solar irradiation. Band edge engineering has thus become a central objective in photocatalyst design. Density Functional Theory (DFT) has been instrumental in predicting and tuning band edge positions across various catalytic systems. For example, dual-atom catalysts (DACs) supported on graphitic carbon nitride (gCN) were systematically screened for HER activity under varying pH conditions. Parameters such as the Gibbs free energy of hydrogen adsorption ( $\Delta G_{H^*}$ ) and electronic descriptors ( $\phi$ ) confirmed the ideal redox compatibility of these DACs, along with low kinetic barriers for HER (Liu *et al.*, 2024). In another prominent study, molybdenum disulfide (MoS<sub>2</sub>) polymorphs underwent substitutional doping with elements like Al, Co, N, and Ni, which effectively tuned the band edges while reducing  $\Delta G_{H^*}$ , thereby enhancing HER activity within the optimal redox window (Eidsvåg *et al.*, 2023).

Two-dimensional (2D) heterostructures offer further control over band alignment through layered design. Heterogeneous 2D transition metal dichalcogenide (TMD) bilayers, such as NbS<sub>2</sub>/HfSe<sub>2</sub> and TaS<sub>2</sub>/HfSe<sub>2</sub>, exhibited excellent HER activity by aligning their CBMs with the hydrogen reduction potential. These configurations were validated through high-throughput DFT simulations and interlayer adhesion energy descriptors (Noh *et al.*, 2018). Photocatalysts based on Co-P@MoS<sub>2</sub> also demonstrated ideal band edge separation, with HER and OER occurring at distinct sites. Partial density of states and charge density difference analysis confirmed that the CBM was positioned to drive HER, while the VBM remained sufficiently positive to facilitate OER (Ma *et al.*, 2023).

Notably, metal-free catalysts such as SiC<sub>3</sub>-doped silicene have shown promise for HER, achieving a near-zero  $\Delta G_{H^*}$  value of 0.008 eV. The substitutional doping induced significant charge transfer and Fermi level alignment, highlighting the effectiveness of band structure modulation in silicon-based materials (Hossain *et al.*, 2025). Band alignment strategies are equally essential for spontaneous overall water splitting (OWS). In boron phosphide (BP) nanowires, nanostructuring induced an indirect-to-direct bandgap transition and favorably aligned the CBM and VBM with HER and OER potentials. Ga doping further improved OER

performance by modifying the band edges (Gajaria *et al.*, 2020).

## 7.2. Reaction Pathway Simulations

Simulating the full reaction pathways of the hydrogen evolution reaction (HER) and oxygen evolution reaction (OER) is essential for understanding catalytic mechanisms at the atomic scale. Density Functional Theory (DFT) serves as a powerful tool to model adsorption energies, intermediate species, and changes in Gibbs free energy, thereby revealing the thermodynamic and kinetic profiles of catalytic processes. This detailed analysis allows researchers to identify favorable active sites, quantify energy barriers, and determine the rate-limiting steps of water splitting reactions. A comprehensive DFT study on Fe-Cu chalcogenide clusters traced the complete mechanistic pathway for overall water splitting. The HER was found to proceed through hydride ( $H^*$ ) intermediates at both metal and chalcogenide centers, whereas the OER followed a low-barrier route via  $OOH^*$  intermediates localized on cobalt and iron selenide complexes. By applying transition state theory, the study mapped energy barriers for each elementary step and quantified the efficiency of bifunctional catalysis (Uzunova, Georgieva, & Zahariev, 2023). In another study, Mo-doped  $NiSe_2-CoSe_2$  heterostructure aerogels were evaluated, showing that Mo substitution significantly enhanced adsorption of  $H^*$  and  $OH^*$  intermediates. The  $\Delta G_{H^*}$  for HER was substantially reduced, while the overpotential for OER decreased to 270 mV, confirming dual-function catalytic behavior (Liu *et al.*, 2023).

A separate investigation on  $CoMoO_4$  demonstrated that its (110) A crystal facet possesses a  $\Delta G_{H^*}$  of 0.22 eV—comparable to platinum—due to a hydrogen bonding geometry involving dual surface oxygen atoms. This facet also exhibited low OER overpotential, suggesting facet-selective synthesis as a viable strategy to design more efficient electrocatalysts (Geng *et al.*, 2023). A systematic study of  $FeNi@Mo_2TiC_2T_x$  MXene nanocomposites further highlighted the impact of interfacial charge transfer. Electron accumulation at Mo-Ni interfacial sites stabilized  $H^*$  and  $OOH^*$  intermediates, thereby facilitating both HER and OER reactions with lower Gibbs free energy requirements (Wang *et al.*, 2021).

In the case of cobalt pentapyridyl molecular catalysts, a combined DFT and *ab initio* molecular dynamics (AIMD) approach revealed a sequential electron-proton transfer pathway for HER. The second protonation step emerged as the rate-limiting step due to steric hindrance around the cobalt center, underscoring the critical role of ligand geometry in hydrogen evolution efficiency (Kiser & Gurdal, 2025). Recognizing the limitations of the computational hydrogen electrode (CHE) model, Gai *et al.* (2020) proposed an expanded free energy landscape using Co- and Fe-doped nitrogen-graphene. This more comprehensive model incorporated

multiple intermediate states and transitions, demonstrating that overpotentials can be misrepresented if single-path assumptions are used. For MOF-derived  $PdNiCo@N$ -doped graphene catalysts, trace Pd incorporation optimized  $H^*$  binding energy ( $\sim 0.02$  eV), aligning with Sabatier's principle and supporting efficient hydrogen desorption. DFT simulations confirmed the improved HER kinetics of the core-shell structure due to balanced intermediate stabilization (Xu *et al.*, 2020). Finally,  $Rh@C_8N_8$  single-atom catalysts showed excellent bifunctional activity, with low HER and OER barriers ( $\Delta G_{H^*} = 0.08$  eV;  $\eta = 0.49$  V). Bader charge and d-band center analyses linked charge redistribution to enhanced binding of key intermediates (Chen *et al.*, 2021).

## 7.3. Catalyst Stability and Surface Engineering

Designing catalysts for water splitting applications requires balancing high catalytic activity and long-term operational stability, especially under harsh or industrial conditions. While noble metals like platinum offer exceptional hydrogen evolution reaction (HER) performance, their high cost and limited durability across pH environments hinder their large-scale adoption. Density Functional Theory (DFT) has become instrumental in understanding and improving catalyst stability by simulating adsorption energies, electronic structures, and surface reconstruction phenomena. A prime example of this approach involves vacancy-engineered transition metal single atoms anchored on CuS substrates. DFT simulations revealed that  $Ti@CuS$  and  $Co@CuS$  configurations exhibit nearly ideal hydrogen adsorption free energies ( $\Delta G_{H^*}$  of 0.01 eV and  $-0.03$  eV, respectively), indicating excellent HER activity. These dopants also bind strongly to surface vacancies, enhancing resistance to structural degradation under long-term electrochemical cycling (Yang *et al.*, 2022). Surface reconstruction is another vital mechanism that activates and stabilizes catalytic sites. In  $CoNiP@Ni_2P$  nanoarrays, dynamic restructuring into oxygen-rich  $CoNiOOH$  phases during OER operation significantly improved performance. DFT modeling confirmed that such reconstructed surfaces optimize the adsorption of reaction intermediates, thereby boosting kinetics and maintaining catalyst integrity (Mao *et al.*, 2024). Stability enhancements have also been realized through alloy design and carbon support frameworks. Ruthenium-nickel-cobalt ( $RuNiCo$ ) alloy nanoparticles embedded in carbon microtubes demonstrated prolonged durability over 30 hours of operation. DFT results indicated that Ru atoms adjust hydrogen adsorption energetics at Ni/Co sites while the carbon shell suppresses corrosion and structural failure (Xue *et al.*, 2022). Amorphous-crystalline heterojunctions, such as those in  $CrS/CoS_2$  composites, offer an effective pathway to synergize reactivity and robustness. Here, amorphous regions introduce highly active sites while crystalline domains resist corrosion. Charge redistribution at the interface tunes the d-band center and stabilizes key intermediates

like  $H^*$  and  $OOH^*$ , leading to enhanced dual-functionality for HER and OER (Lu *et al.*, 2023).

Interface engineering is further exemplified in  $CrOx-Ni_3N$  heterostructures, where the coupling of amorphous  $CrOx$  with crystalline  $Ni_3N$  results in efficient HER activity. DFT studies confirmed that interfacial electron transfer reduces barriers for both water dissociation and hydrogen adsorption. Additionally, oxygen vacancies within  $CrOx$  contribute to long-term durability under alkaline environments (Yang *et al.*, 2022). A multi-metallic strategy was adopted in  $RuCoNiP@Ni(OH)_2$  catalysts, where in situ reconstruction during operation generated  $Ni/Co-OH$  interfacial sites. DFT revealed that Ru doping modulates the Ni d-band near the Fermi level, reducing energy barriers for hydrogen evolution and maintaining robust structural stability throughout cycling (Lian *et al.*, 2024).

In  $FeNbO_{4-x}@NC$  systems, integrating nitrogen-doped porous carbon matrices and oxygen vacancies improved electrical conductivity and reduced adsorption barriers for  $H^*$  and  $OH^*$  species. These engineered defect sites localized charge carriers, enhancing HER and OER efficiency and extending catalyst lifespan (Fu *et al.*, 2024). Another innovative strategy involved La-doped  $RuO_2$ , where aliovalent doping and oxygen vacancy creation synergistically modulated the Ru d-band center. DFT simulations showed enhanced binding of OER intermediates and improved acid corrosion resistance, enabling over 500 hours of stable activity in acidic environments (Wu *et al.*, 2022). Finally, ZIF-67-derived  $Ni/Co@NC$  catalysts doped with trace Ru demonstrated that even minimal noble metal incorporation can introduce additional active sites and reduce water dissociation barriers. DFT modeling corroborated the enhanced HER and OER activity and highlighted the stabilizing role of nitrogen-doped carbon supports (Salah *et al.*, 2024).

## 8. Environmental Impact Assessment via DFT:

### 8.1. Toxicity Predictions of Material Components

Accurate environmental risk assessments of emerging materials, particularly those used in electronics, energy storage, and catalysis, demand advanced computational methods to predict toxicity. Density Functional Theory (DFT) provides a powerful molecular-scale approach to understanding how material components interact with biological systems and the environment, primarily through mechanisms involving reactive oxygen species (ROS). ROS formation is often linked to regions of high electron density and unbalanced charge distribution, particularly around transition metals and reactive heteroatoms. One example is the degradation of sulfamethoxazole via electrochemical oxidation, where DFT analysis identified aromatic and isoxazole ring structures as susceptible to ROS attack. This computational prediction was supported by experimental detection of intermediates, confirming the

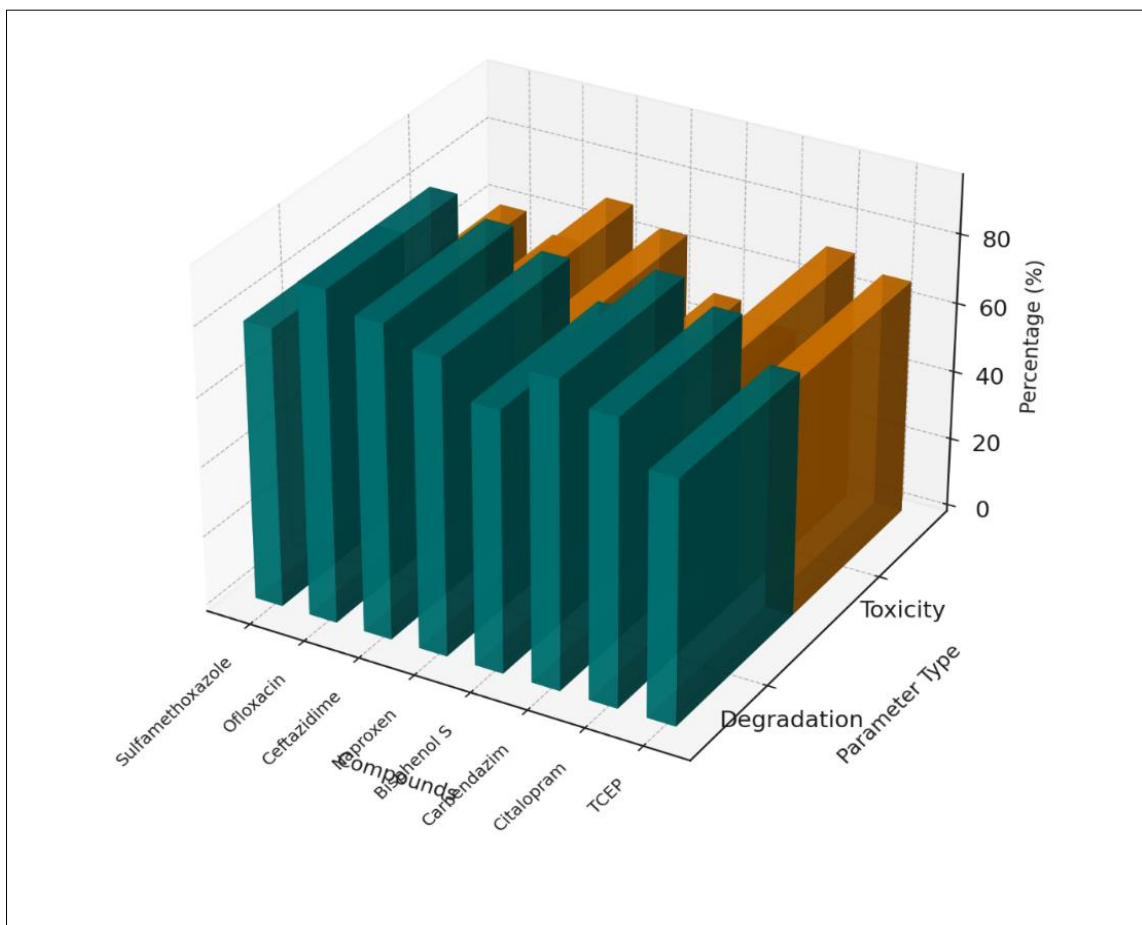
correlation between molecular orbital characteristics and degradation pathways (Hai *et al.*, 2020). Similarly, in the treatment of pharmaceutical wastewater containing ofloxacin, DFT-based Fukui function analysis revealed key electrophilic attack sites at C14, C15, and C23 on the molecule. These sites corresponded to the most reactive regions during ROS-driven degradation using a  $CuFe-ZnO$  catalyst system. Further quantitative structure-activity relationship (QSAR) modeling demonstrated a significant decrease in mutagenicity and bioaccumulation potential after treatment (Kumar *et al.*, 2024). Heavy metals such as lead (Pb) and cadmium (Cd) present persistent environmental and biological hazards. Their toxicological behavior is often tied to redox activity and electron affinity. DFT models have been widely applied to simulate these elements' charge distribution and ROS-generating tendencies, explaining their propensity to cause DNA damage and oxidative stress through electron imbalance and redox cycling (Syed, Kapoor, & Bhat, 2018).

In another study, the degradation of ceftazidime—a cephalosporin antibiotic—was modeled using DFT and verified by HPLC-MS. While overall mineralization proceeded efficiently, key intermediate byproducts such as aminothiazole and pyridine rings retained moderate to high toxicity. These findings emphasized the need for complete degradation to avoid secondary environmental risks (Duan *et al.*, 2020). Likewise, in the oxidative degradation of naproxen, a common non-steroidal anti-inflammatory drug (NSAID), DFT simulations revealed that hydroxyl radical attack formed intermediates with greater molecular reactivity and lower HOMO-LUMO energy gaps than the parent molecule. These intermediates were confirmed to be initially more toxic in *E. coli* bioassays, although complete mineralization led to detoxification (Feng *et al.*, 2023).

Fluoroquinolone antibiotics also exhibit transformation into harmful byproducts under UV-based oxidation. DFT analyses of bond dissociation energies and Fukui indices highlighted that methoxy and piperazine substituents significantly influence degradation pathways and the toxicity of resulting intermediates (Sun *et al.*, 2024). Endocrine-disrupting compounds like bisphenol S (BPS) have also been studied using DFT. Hydroxylation at ortho-carbon sites was predicted as the key degradation step, validated by  $Co_3O_4$ -activated peroxymonosulfate oxidation experiments. Most of the resulting byproducts showed lower predicted eco-toxicity than the parent compound (Wang *et al.*, 2022). DFT-assisted degradation modeling suggested routes involving decarboxylation and nucleophilic substitution for fungicides such as carbendazim. These predicted pathways generally yielded less toxic products, reinforcing the role of computational chemistry in identifying safer remediation strategies (Liu *et al.*, 2022). Additionally, UV oxidation of antidepressants like citalopram and venlafaxine

showed that certain photolysis products were more toxic than the original compounds. DFT-based pathway analysis and toxicity evaluation revealed the risk of incomplete oxidation during wastewater treatment (Lin *et al.*, 2022). Lastly, tris(2-chloroethyl) phosphate (TCEP), a widely used organophosphate flame retardant, was studied using DFT to model oxidative degradation

by ultrasound-assisted Fenton (US/Fenton) chemistry. Hydroxyl radicals ( $\cdot\text{OH}$ ) were identified as the primary oxidants, driving bond cleavage. Most degradation products exhibited reduced toxicity, although a few intermediates remained of moderate concern (Zhang *et al.*, 2024).



**Graph: 3D Comparison of DFT-Predicted ROS Degradation and Toxicity Reduction for Emerging Pollutants**

## 8.2. Environmental Degradation Pathways

Understanding pollutant degradation under environmental conditions is essential for predicting the toxicity of byproducts, refining remediation strategies, and advancing photocatalyst design. Density Functional Theory (DFT), often integrated with experimental tools such as liquid chromatography-mass spectrometry (LC-MS) and molecular dynamics (MD), has become fundamental in simulating key processes such as photolysis, oxidation, and advanced degradation mechanisms in both natural and engineered systems. One of the most robust approaches to modeling environmental degradation involves simulating singlet oxygen ( $^1\text{O}_2$ )-mediated oxidation, a highly selective pathway typically initiated by photocatalysts or activated persulfates. DFT studies have demonstrated that molecular reactivity indicators such as HOMO–LUMO energy gaps and Fukui indices effectively predict the vulnerability of pollutants to electrophilic attack and

single-electron transfer processes, enhancing our understanding of  $^1\text{O}_2$  reactivity in diverse matrices (Rayaroth *et al.*, 2023). Photolytic degradation under ultraviolet radiation has also been extensively investigated using DFT. In compounds such as carbamazepine (CBZ) and caffeine, DFT combined with frontier molecular orbital theory identified the most reactive sites—such as C(7C), N(17N), and O(18O) in CBZ and C(9C) in caffeine—as susceptible to attack by hydroxyl and singlet oxygen radicals, aligning well with experimental degradation patterns (Liu *et al.*, 2022).

Solar-driven photocatalysis has been intensively modeled for phenolic pollutants, particularly when using  $\text{TiO}_2$  immobilized on different substrates. One study showed  $\text{TiO}_2/\text{glass}$  composites exhibited the highest degradation efficiency under solar light. DFT simulations provided critical insights into the catalyst–substrate interaction energies and surface activation

mechanisms, validating the observed degradation kinetics (Silerio-Vázquez *et al.*, 2022). Similarly, advanced oxidation processes like solar photoelectro-Fenton (SPEF) have benefited from DFT-supported mechanistic understanding. DFT helped elucidate bond dissociation energies for recalcitrant organic pollutants, supporting MS-verified degradation intermediates and confirming hydroxyl radical attack as the dominant pathway (Brillas, 2023). DFT and molecular dynamics were successfully combined in the study of pindolol photodegradation. The reactive hydroxyl groups on the indole ring were identified as key intermediates through simulations and confirmed experimentally via LC-MS. Follow-up toxicity assays linked these intermediates to adverse cellular outcomes, highlighting DFT's predictive power (Armaković *et al.*, 2020). In another case, photodegradation of ceftriaxone showed faster degradation in ultrapure water than in natural matrices. DFT-derived Fukui indices were used to pinpoint reactive molecular sites, and the data supported a model of matrix-dependent noncovalent interactions influencing degradation kinetics (Abramović *et al.*, 2021).

For chloramphenicol, DFT calculations identified  $\beta$ -C-C bond cleavage as the initial photolysis step, followed by ROS-driven formation of nitrosobenzene and benzoic acid derivatives. These predicted intermediates were validated through experimental tracing, underscoring DFT's reliability in simulating photolytic cascades (Belikov *et al.*, 2024). Ceftazidime degradation under UV-light systems and different anode materials followed DFT-modeled pathways, with hydroxyl radical attack being the primary mechanism. Sodium chloride was found to boost radical formation, and LC-MS-identified intermediates closely matched those predicted computationally (Duan *et al.*, 2020). Finally, in hybrid photocatalyst systems like  $\text{TiO}_2$ -AgNPs, DFT-based electron density mapping revealed interactions between the (101) plane of  $\text{TiO}_2$  and the (111) face of Ag nanoparticles. This interaction reduced the bandgap and promoted visible-light-induced oxidation of ciprofloxacin. Experimentally observed degradation intermediates aligned with the DFT-derived pathways, confirming the method's accuracy in modeling photocatalytic behavior of nanostructured materials (Huerta-Aguilar *et al.*, 2020).

### 8.3. Lifecycle Modeling of Solar Cell Materials

Lifecycle assessment (LCA) has become a cornerstone in evaluating the environmental viability of photovoltaic (PV) technologies. It assesses the total environmental burden of solar materials across all stages—from raw material extraction and manufacturing to usage, recycling, and final disposal. Integrating Density Functional Theory (DFT) with LCA tools has significantly enhanced the ability to model material properties, predict degradation pathways, and optimize energy return and recyclability, thus aiding in sustainable solar cell design. One study on high-concentration

photovoltaic (HCPV) systems incorporating space-grade solar cells and precision micro-tracking optics demonstrated the environmental benefits of component recycling. Through DFT-informed LCA models, it was shown that recycling key materials like polymethyl methacrylate (PMMA), rubber, and electronic parts could reduce the system's carbon footprint by 17%, lowering total emissions from 240 kg to 201 kg  $\text{CO}_2$ -eq over a 25-year operational life. Notably, the energy payback time (EPBT) was reduced to as little as 0.87 years in high-irradiance regions such as Madrid (Ziemińska-Stolarska *et al.*, 2023). In another analysis comparing n-type and p-type silicon modules under the Chinese electricity grid scenario, the polysilicon production phase emerged as the most energy-intensive stage. DFT simulations indicated that adopting renewable electricity sources during wafer fabrication could drastically lower emissions. Moreover, n-type bifacial modules showed better energy return on investment due to their higher efficiency and dual-surface absorption capability (Wang *et al.*, 2024). A comparative lifecycle study of standard passivated emitter and rear contact (PERC) modules and tandem luminescent solar concentrator-PERC modules highlighted how design innovation impacts sustainability. The tandem architecture reduced carbon emissions by over 40%, dropping from 31.3 to 18.0 g  $\text{CO}_2$ /kWh. This improvement was partly due to DFT-guided material modifications, including eliminating toxic antimony compounds and adopting thinner silicon layers (Papaioannou, Singh, & Lee, 2022). Further, in India, the ecological footprint (EFT) of a 1 MW rooftop PV installation revealed that PV modules accounted for nearly 76% of the environmental impact. The calculated EFT was  $1.59 \times 10^5$  gha/kWh, and PV-based electricity led to a ~95% reduction in footprint compared to conventional grid energy. These results underline the role of LCA in quantifying the ecological benefits of solar transitions (Biswas, Husain, & Prakash, 2020). Hybrid concentrator photovoltaic/thermal (CPV/T) systems were also evaluated for lifecycle sustainability. Without recycling, aluminum supports and copper components presented the highest ecological damage scores (DALY = 0.015). Recycling halved the environmental impact and reduced EPBT from 1.6 to 0.6 years (Lamnatou *et al.*, 2018).

Recycling of silicon wafers from end-of-life PV modules has shown promise as a high-value pathway. DFT simulations demonstrated that boron-doped recycled wafers maintained adequate electronic properties when used in perovskite-silicon tandem architectures, offsetting recombination losses due to impurity doping. This strategy was projected to save up to 0.16 kWh/Wp energy during manufacturing (Geerligs, Kuypers, & Theelen, 2024). In Peru, LCA studies of small-scale rooftop systems and large-scale 179.5 MW utility plants confirmed that incorporating recycling stages substantially cut lifecycle carbon emissions by 13% in large plants. EPBT varied between 1.8 and 2.3

years depending on geographic irradiance levels (Cortez *et al.*, 2024). Finally, recent models assessing the economic and environmental outcomes of rooftop concentrator systems with advanced nanomaterials—including perovskites and multi-junction cells—have shown that while these systems have higher initial costs,

they exhibit shorter payback periods and a markedly lower lifecycle carbon footprint. These findings affirm that material innovation, particularly when optimized using DFT, delivers environmental sustainability and long-term economic advantages (Kumar, 2024).

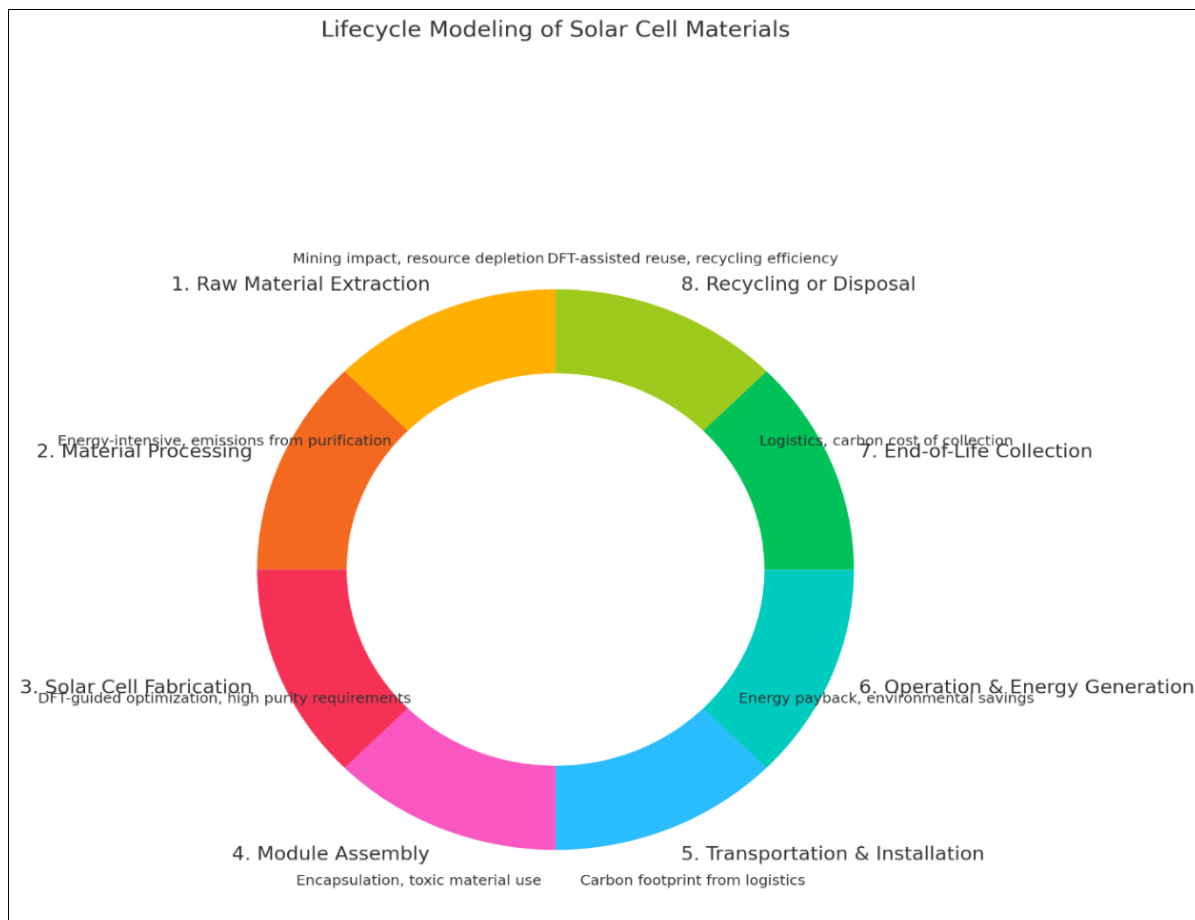


**Figure: Lifecycle Modeling of Solar Cell Materials**

## 9. Advanced Nanomaterials and DFT Modeling:

### 9.1. Quantum Dots and Nano-Heterostructures

Quantum dots (QDs) are zero-dimensional semiconductor nanocrystals characterized by discrete energy levels arising from strong quantum confinement effects. Their unique optical and electronic properties are highly tunable through modifications in size, shape, composition, and the engineering of heterostructures. Density Functional Theory (DFT) has become indispensable for understanding and predicting their bandgap behavior, exciton dynamics, and charge localization, especially in the context of designing nano-heterostructures for applications in optoelectronics, photovoltaics, and photocatalysis. Core-shell QDs, particularly those based on type-I and type-II configurations, are extensively utilized to control carrier recombination and spatial localization. For example, CdSe/ZnS and CdSe/CdTe QDs demonstrate tunable electron-hole separation via shell thickness and core size variations. A theoretical study on CdSe/ZnTe and CdSe/CdTe nanocrystals showed that small core

dimensions favor type-I behavior with localized excitons. In contrast, thicker shells promote type-II alignment, facilitating efficient charge separation across the interface (Aghoutane *et al.*, 2022). Advanced DFT modeling of CdSeS/ZnS nanoplatelets—quasi-2D core-shell systems—revealed precise confinement and band alignment control. DFT simulations demonstrated that approximately 34% of the excited electrons migrate into the ZnS shell, enhancing charge separation and optical performance (Szemjonov *et al.*, 2018). Hybrid nanocrystals such as Au-decorated CdS/ZnS QDs have shown extraordinary photocatalytic enhancement. Incorporating an Au<sub>2</sub>S interfacial layer facilitated rapid charge transfer, with DFT identifying a lowered energy barrier for electron extraction, resulting in a 400-fold increase in hydrogen production (Jin *et al.*, 2023).

DFT studies have also contributed to understanding complex interfacial effects, such as strain-induced band offsets, surface trap states, and carrier lifetimes. A review by Sahu and Kumar (2022)

emphasized the crucial role of theoretical modeling in the photophysical behavior of QDs, particularly for photoluminescence tuning and nonlinear optical responses. In perovskite-based systems, CsPbBr<sub>3</sub> QDs encapsulated within ZnO nanowires exhibited improved luminescence and device longevity. When coupled with embedded gold nanoparticles, the resulting exciton-plasmon interactions yielded a 1.55× increase in electroluminescence, as validated through DFT simulations and time-resolved spectroscopy (Shi *et al.*, 2018). The dynamics of carrier localization were further explored in CdSe–CdS quantum rods. Terahertz pump–probe spectroscopy, supported by DFT, revealed that core-trapped excitons are relatively immobile, while carriers in the shell contribute to conductivity, enhancing their applicability in energy devices (Staechelín *et al.*, 2022). Investigations into alloyed II–VI QDs, such as ZnTe/CdSe, showed that charge transfer and bandgap behavior strongly depend on compositional gradients at the core–shell interface. X-ray absorption spectroscopy (XAS) combined with DFT confirmed the presence of Cd<sub>x</sub>Zn<sub>1-x</sub>Te cores and CdSe shells, underscoring the need for precise interface engineering (Gentle *et al.*, 2019). In hybrid photodetectors, MoS<sub>2</sub> nanosheets coupled with InP/ZnS or InP/CdS QDs demonstrated improved responsivity due to optimized energy band alignment. DFT-guided design revealed that thicker type-II shells minimized recombination by tailoring interfacial potential barriers (Chang *et al.*, 2021). Similarly, GaAs/AlGaAs core–multishell nanowires embedded with quantum wells achieved extended photoluminescence lifetimes. DFT calculations showed that the multilayer architecture enhanced confinement and reduced surface recombination, which is critical for efficient light-emitting devices (Zhou *et al.*, 2019). Lastly, ZnWO<sub>4</sub>–SnO<sub>2</sub> core–shell nanorods exemplify heterostructure synergy for visible-light photocatalysis. DFT modeling confirmed effective charge separation, bandgap narrowing, and improved redox performance, making them viable for next-generation solar-driven systems (Babu *et al.*, 2023)

## 9.2. Plasmonic Nanoparticles in Photovoltaics and Remediation

Plasmonic nanoparticles, especially those made from noble metals such as gold (Au), silver (Ag), and platinum (Pt), have emerged as transformative agents in solar energy harvesting and environmental remediation. Their ability to support localized surface plasmon resonances (LSPR)—coherent oscillations of conduction electrons induced by light—enhances light absorption, hot electron generation, and catalytic activity. DFT modeling provides a molecular-level understanding of these phenomena, particularly regarding energy band modulation, Schottky barrier formation, and electron transfer kinetics. A fundamental breakthrough in the field was demonstrating that Au@Pt core-shell nanoparticles enhance catalytic activity via plasmonic hot electron "painting." Upon LSPR excitation, Au nanoparticles generate hot electrons that reduce Pt

precursors to form an asymmetric Pt shell. DFT modeling confirmed synergistic electron redistribution at the interface, enhancing H<sub>2</sub>O<sub>2</sub> reduction and overall electrocatalytic sensitivity (Xia *et al.*, 2022). Plasmonic Ag–Au alloy nanoparticles supported on TiO<sub>2</sub> demonstrate a unique strategy to fine-tune the LSPR energy and catalytic response. A volcano-type relationship between the Ag: Au ratio and photocatalytic water oxidation activity was observed. DFT and photoemission spectroscopy jointly confirmed that variations in d-band onset energy and electric field localization are responsible for the enhanced interfacial charge separation (Haider *et al.*, 2021). Hot-electron injection was also validated on TiO<sub>2</sub> nanotube arrays decorated with Au nanoparticles, where the size-dependent decay of LSPR led to oxygen evolution via enhanced charge separation. DFT simulations demonstrated that smaller Au particles reduce the Schottky barrier, enhancing hot carrier transfer and surface photovoltage response (Moon *et al.*, 2018). Au@CuS core-shell nanoparticles are examples of dual-plasmonic systems that combine LSPR from noble metals and valence band hole oscillations from doped semiconductors. DFT modeling and spectroscopy confirmed selective energy coupling into both plasmonic components, enabling wavelength-specific modulation of photocatalytic and photothermal effects (Sun *et al.*, 2020).

Pt-decorated MIL-53 MOFs supported on TiO<sub>2</sub> formed hybrid catalysts exhibiting both Schottky junction formation and LSPR-induced hot electron transfer. DFT simulations confirmed the role of noble metal Fermi-level tuning in enhancing electron injection, which improved ketoprofen degradation and minimized electron–hole recombination (Zhao *et al.*, 2022). ZnO–CdS–Au nanorod heterojunctions showed that LSPR in Au greatly enhanced water splitting efficiency. The system achieved a 235% improvement in photoconversion efficiency over the binary ZnO–CdS structure. DFT analysis linked this enhancement to reduced recombination and efficient directional migration of hot electrons across the ternary interface (Ma *et al.*, 2019). Full-spectrum plasmonic semiconductors are emerging as noble-metal-free alternatives with tunable LSPR features. Heavily doped oxides like W: WO<sub>3</sub> and Tin mimic noble metals' behaviour while offering lower cost. DFT calculations validated the presence of depletion layers that hinder carrier transfer, and surface modification strategies were proposed to resolve this limitation (Liu *et al.*, 2024). In a key study on Au–TiO<sub>2</sub>–Pt nanodumbbells, simultaneous longitudinal and transverse plasmon excitation produced energetic hot carriers that were injected into TiO<sub>2</sub> and enhanced H<sub>2</sub> evolution by over fourfold. DFT and finite-difference time-domain (FDTD) simulations supported the correlation between plasmon decay and electric field enhancement around Au nanorods (Zhu *et al.*, 2020). Lastly, advanced optical sensors using Au@AuY/Au

core-shell nanoparticles have shown tunable nonlinear optical properties. DFT and Mie theory revealed how size-dependent LSPR behavior is linked to the quantum size effect and free electron density modulation, leading to enhanced third-order nonlinearities critical for ultrafast optoelectronic devices (Liu *et al.*, 2023).

### 9.3. 2D Materials for Dual Applications

Two-dimensional (2D) materials such as molybdenum disulfide (MoS<sub>2</sub>) and graphitic carbon nitride (g-C<sub>3</sub>N<sub>4</sub>) have emerged as multifunctional platforms due to their exceptional optoelectronic, photocatalytic, and structural properties. These materials are particularly effective in dual applications such as solar energy harvesting and environmental remediation. Density Functional Theory (DFT) plays a pivotal role in predicting and optimizing their performance by enabling bandgap engineering, charge transport simulations, and interfacial property analyses. MoS<sub>2</sub>, a prototypical transition metal dichalcogenide (TMD), offers tunable electronic structures and a high surface-to-volume ratio, making it suitable for efficient charge generation and transport. In a recent DFT-guided study, FeS/MoS<sub>2</sub> heterostructures were designed to introduce sulfur vacancies and intrinsic electric fields, enhancing electron mobility. This structure demonstrated a 3.77-fold improvement in Cr(VI) photocatalytic reduction compared to pristine MoS<sub>2</sub> (Liu *et al.*, 2024). Another class of Mo-based materials, MoO<sub>3-x</sub>S<sub>x</sub>/MoS<sub>2</sub> heterostructures, exhibited a transition from Type-III to Type-II band alignment upon sulfur doping. Using HSE06 functionals in DFT calculations, the heterojunction was optimized for spatial electron-hole separation—ideal for Z-scheme water splitting configurations (Shahrokhi *et al.*, 2021). Ni-doped MoS<sub>2</sub> in layered Ni-MoS<sub>2</sub>/g-C<sub>3</sub>N<sub>4</sub> composites further extends dual-functionality. These heterostructures enable both hydrogen evolution and Cr(VI) detoxification, achieving over 29% quantum yield. DFT and gas-phase tracking confirmed that Ni-doping increases interfacial carrier density and improves water oxidation kinetics (Koutsouroubi *et al.*, 2021). Hybrid 0D/2D architectures, such as graphene quantum dots (GQDs) integrated with MoS<sub>2</sub>, exhibit tunable band alignment. DFT modeling showed that size control of GQDs enables a transition from Type-I to Type-II alignment, thereby improving visible-light-driven hydrogen evolution (Luo *et al.*, 2022).

Superlattice-like heterostructures formed by intercalating g-C<sub>3</sub>N<sub>4</sub> with 2H-MoS<sub>2</sub> provide nanoscale confined channels for charge transfer. DFT simulations revealed that interlayer electron-electron interactions, rather than dielectric effects, enhanced MoS<sub>2</sub> conductivity and HER performance. These structures delivered low overpotentials and high exchange current densities, indicative of efficient hydrogen evolution (Gan *et al.*, 2024). Janus MoSSe integrated into van der Waals heterostructures with MoS<sub>2</sub> enables Z-scheme charge transfer. Using GW-corrected DFT calculations, these

systems exhibited excellent hydrogen evolution reaction (HER) activity, strong visible light absorption, and reduced recombination rates due to favorable H<sub>2</sub>O adsorption energy (Singh *et al.*, 2020). Co<sub>9</sub>S<sub>8</sub>-MoS<sub>2</sub> heterostructures represent another innovative system, where covalent bonding induces charge redistribution from Co to Mo, making Mo sites electron-rich. This configuration achieved superior HER activity under acidic, neutral, and alkaline conditions, even outperforming Pt/C in some cases (Kim *et al.*, 2020). For optoelectronic and photovoltaic applications, BSe-MoS<sub>2</sub>/WS<sub>2</sub> heterostructures were identified as efficient Type-II systems with low lattice mismatch. DFT models predicted power conversion efficiencies up to 19.3%, especially under optimized strain and external electric field conditions (Li *et al.*, 2021). A large-scale computational screening of over 200,000 2D heterostructures using DFT and the Anderson rule revealed that MoS<sub>2</sub>-based systems predominantly exhibit Type-II alignment. These characteristics make them ideal for hydrogen evolution, water splitting, and high-performance photodetectors (Choudhary *et al.*, 2020).

## 10. Machine Learning Integration with DFT:

### 10.1. Accelerated Material Discovery

The integration of machine learning (ML) with Density Functional Theory (DFT) has significantly accelerated the discovery and optimization of functional materials. By leveraging large DFT-generated datasets, researchers are training surrogate models that replace computationally expensive first-principles calculations, enabling rapid screening across vast compositional and structural design spaces. This synergy is central to the emerging field of materials informatics, aligning with the goals of the Materials Genome Initiative. A foundational application of DFT-ML integration involved the discovery of redox-active organic electrode materials. Machine learning models such as kernel ridge regression, Gaussian processes, and deep neural networks were trained to predict redox potentials with remarkable accuracy (~0.1 V deviation). Active learning techniques and high-throughput workflows ensured that only the most promising candidates were prioritized for full DFT calculations, significantly accelerating the design cycle of next-generation battery materials (Allam *et al.*, 2022).

In the search for superhard materials, Fan *et al.* (2024) employed high-throughput DFT computations combined with support vector regression, random forest, and neural networks. These models were trained on structural and mechanical datasets to predict the bulk and shear moduli of over 1,200 carbon allotropes within the Pca<sub>21</sub> symmetry group. Eight novel allotropes were discovered and subsequently validated through DFT analysis, demonstrating the power of ML in guiding mechanical property predictions. The DARWIN framework represents a notable advancement in interpretable deep learning for materials discovery. Trained on hybrid-functional DFT data, DARWIN couples ML with evolutionary algorithms to conduct

property-driven searches across an enormous space of ternary ( $10^8$ ) and quaternary ( $10^{11}$ ) compounds. This approach successfully identified previously unknown wide-bandgap UV-emitting semiconductors that were later experimentally synthesized (Choubisa *et al.*, 2021).

In another innovative strategy, researchers explored the Si–C–N ternary system using a hybrid methodology combining DFT, evolutionary algorithms, and machine learning. Surrogate models were trained on hardness and formation energy landscapes to rapidly identify ceramics with optimized thermal and mechanical properties suitable for high-temperature applications (Bavdekar *et al.*, 2023). The application of ML in thermoelectric materials design has also shown

tremendous promise. Curated high-throughput databases enabled the training of regression models capable of accurately predicting key transport properties such as Seebeck coefficient, electrical conductivity, and lattice thermal conductivity. These ML tools helped reduce the candidate pool by orders of magnitude while retaining accuracy, greatly facilitating the discovery of efficient thermoelectric materials (Juneja & Singh, 2021).

Overall, the convergence of ML and DFT has established a new paradigm in materials discovery—one where data-driven modeling, high-throughput simulation, and physical theory coalesce to enable faster, more targeted exploration of complex material systems.

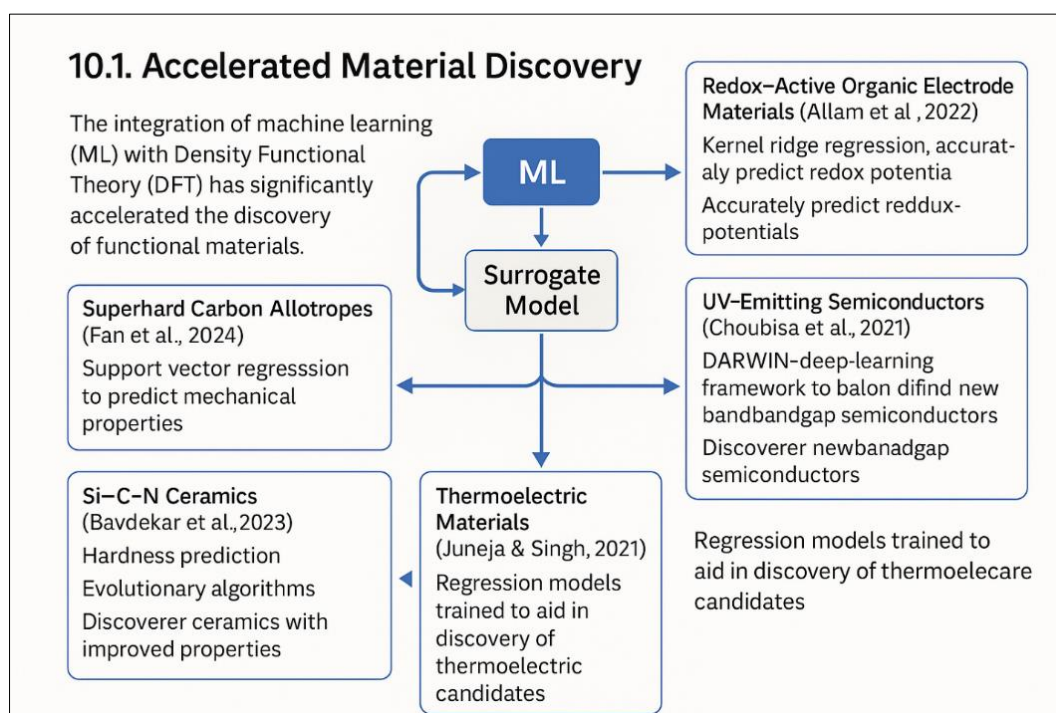


**Figure: "Synergistic Integration of Machine Learning and DFT in Accelerated Materials Discovery"**

## 10.2. Feature Selection and Model Training for DFT Outputs

The successful integration of machine learning (ML) with Density Functional Theory (DFT) strongly depends on engineering accurate, physically meaningful descriptors and selecting appropriate regression models. Descriptors—quantitative features that capture the chemical, structural, or electronic properties of materials—form the foundation for predictive modeling. Their choice directly impacts model accuracy, interpretability, and generalizability.

One of the key challenges in materials informatics is reducing the dimensionality of descriptor space while preserving predictive power. A novel two-level ensemble feature selection approach was developed for bispectrum descriptors used in the Spectral Neighbor Analysis Potential (SNAP) framework. This method

combines perturbation-based filtering with ensemble statistical selection, resulting in 30% lower prediction complexity and 50% faster model training, with no compromise in the accuracy of atomic energy predictions for transition metals like Fe, Ni, Cu, and Mo (Jiang *et al.*, 2023). High-dimensional DFT datasets often contain redundant or correlated features. Recursive feature elimination and correlation-based filtering have proven effective in refining these input spaces. In one study, extreme gradient boosting models were trained on 12-dimensional adsorption energy descriptors. These were reduced to just two core features without any performance loss—an approach particularly suited for small datasets (Hu *et al.*, 2024). In perovskite oxide studies, machine learning models trained on descriptors derived from elemental properties and DFT-computed energies strongly predicted thermodynamic stability. Regression models applied to over 1,000 perovskite compounds achieved high accuracy in estimating

formation energies and hull stability, demonstrating the value of feature selection in compositional spaces (Li *et al.*, 2018).

Descriptor optimization also plays a critical role in polymer electronics. Support vector regression (SVR) models were trained using 16 chemically intuitive descriptors selected via the maximum relevance and minimum redundancy (mRMR) algorithm. These included molecular polarity, aromaticity, and backbone conjugation, yielding highly interpretable models with external  $R^2$  values exceeding 0.92 (Xu *et al.*, 2021). In developing orbital-free DFT, predicting kinetic energy densities (KED) from electron density distributions requires finely tuned local descriptors. Gaussian process regression models trained on smoothed fourth-order gradient expansion terms were able to capture KED behavior accurately, even when trained on only 0.3% of total DFT datasets for elements like Al, Si, and Mg, demonstrating data efficiency and low overfitting (Manzhos *et al.*, 2023). Machine learning and symbolic regression were also used to predict molecule–surface adsorption interactions in low-dimensional materials. Automatically generated hybrid descriptors such as polarizability and bond types enabled high-accuracy predictions with minimal training data, emphasizing the value of innovative feature generation techniques (Hu & Zhang, 2023). Finally, interpretable ML models have benefited from decision tree–based feature ranking augmented by expert-driven weighting schemes. In systems involving perovskites and rare-earth alloys, this strategy enabled the selection of a small, optimized set of descriptors that accurately classified material stability and electronic properties with over 90% accuracy (Selvaratnam *et al.*, 2023).

### 10.3. AI-Guided Stability and Efficiency Predictions

Integrating artificial intelligence (AI) with DFT has enabled rapid and accurate thermodynamic stability and device efficiency prediction, especially in materials screening and inverse design. Surrogate models—trained ML representations of DFT computations—are at the heart of this progress, making it possible to optimize material properties across vast compositional spaces with minimal computational cost. One standout example is the DARWIN model, an interpretable deep learning system trained on high-throughput hybrid DFT data to predict structural stability and band gaps. It employs an evolutionary search algorithm to identify UV-emitting semiconductors, successfully predicting and validating  $K_2CuX_3$  ( $X = Cl, Br$ ) as new direct bandgap materials, illustrating the power of surrogate models in guiding synthesis-ready candidates (Choubisa *et al.*, 2021). In the field of halide perovskites, a multi-fidelity machine learning framework combined with a genetic algorithm (GA) was used to screen over 150,000  $ABX_3$  compositions. Surrogate models trained on decomposition energy and bandgap data successfully guided the discovery of new stable, high-efficiency

candidates with predicted photovoltaic efficiencies >15% (Yang *et al.*, 2024).

For high-temperature ceramics, surrogate models were trained on DFT-calculated stability and hardness metrics to explore the Si–C–N design space. These models allowed accelerated prediction of formation energy and mechanical performance, reducing the need for exhaustive DFT runs while maintaining predictive accuracy (Bavdekar *et al.*, 2023). Energy above hull (E<sub>hull</sub>) predictions for  $ABO_3$  perovskites were achieved using a PSO-optimized support vector regression (SVR) model trained on multi-scale descriptors. This surrogate model effectively predicted thermodynamic stability and screened numerous new candidates from the Materials Project database (Chen *et al.*, 2022). A separate study used a neural network-based surrogate model to design transition metal complexes with optimized redox potential and solubility. The model incorporated uncertainty quantification via efficient global optimization (EGO), allowing rapid convergence toward Pareto-optimal materials for redox flow batteries—achieving a 500× speed-up compared to random search (Janet *et al.*, 2020). Surrogate models also contributed to efficient hydrogen evolution catalyst discovery. A review highlighted how ML-assisted DFT methods—including random forests and generative adversarial networks—were used to predict catalytic activity and structural stability of single-atom catalysts, optimizing reaction pathways while drastically reducing computational time (Yu *et al.*, 2025). In computational molecular design, Gaussian process regression (GPR) surrogates were deployed to predict molecular properties such as lattice energy and phase stability, enabling accurate black-box optimization of organic crystals with only a fraction of the full DFT dataset (Bowskill *et al.*, 2020). Graph-based deep learning, combined with variational autoencoders and crystal relaxation methods like M3GNet, has also enabled AI-assisted discovery of porous oxides for energy storage. Surrogates screened low-formation-energy structures and predicted high-stability candidates for multivalent-ion batteries (Datta *et al.*, 2024).

## 11. Challenges and Limitations of DFT:

### 11.1. Accuracy vs. Computational Cost Trade-offs

The trade-off between computational efficiency and predictive accuracy remains a fundamental challenge in DFT. Local and semi-local exchange-correlation functionals such as the Local Density Approximation (LDA) and Generalized Gradient Approximation (GGA) offer fast calculations but often neglect nonlocal correlations and suffer from self-interaction errors, especially in open-shell systems and transition metal complexes (Najibi & Goerigk, 2018).

Hybrid functionals like B3LYP and HSE06 partially address these limitations by incorporating exact exchange, significantly improving electronic property predictions. However, they incur substantially higher

computational costs, particularly for large molecular or periodic systems. The cubic or worse scaling behavior of these methods often results in prohibitive runtime and memory demands. For example, linear-scaling DFT has been applied to simulate large metal–DNA complexes (~1000 atoms), where dispersion-inclusive functionals improved realism but introduced notable convergence difficulties in biologically relevant environments (Ortiz de Luzuriaga *et al.*, 2022). To balance efficiency and accuracy, newer functionals like B97M-V and  $\omega$ B97M-V implement nonlocal van der Waals corrections as additive, post-self-consistent energy terms. These approaches allow for improved interaction modeling without full iterative inclusion, reducing cost while maintaining accuracy (Najibi & Goerigk, 2018).

## 11.2. Limitations in Long-Range Interactions and Excited States:

DFT's conventional functionals are notoriously inadequate at capturing long-range dispersion interactions, such as van der Waals (vdW) forces. This shortfall leads to significant underestimation of binding energies in weakly interacting systems. Studies on molecular physisorption on graphene surfaces have demonstrated the necessity of vdW-inclusive functionals to account for many-body effects and screening contributions for accurate modeling (Silvestrelli, 2021).

Modeling excited states introduces further complications. Although Time-Dependent DFT (TDDFT) is widely used for photophysical and photochemical predictions, it struggles with describing charge-transfer excitations and double excitations. For instance, in MR-TADF molecules, TDDFT consistently overestimates singlet-triplet gaps ( $\Delta E_{ST}$ ) due to poor electron correlation treatment, requiring higher-level methods like SCS-CC2 for reliable accuracy (Hall *et al.*, 2021). In donor–acceptor systems, excited-state charge transfer is strongly influenced by solvent environments. TDDFT predictions for such systems often depend heavily on the chosen functional and require the use of range-separated hybrid functionals for proper energy alignment and charge localization (Ahmed & Manna, 2020).

## 11.3. Issues with Realistic Environmental Conditions

Standard DFT is fundamentally a zero-Kelvin, vacuum-based formalism, making it poorly suited for modeling systems under realistic environmental conditions without explicit corrections. Solvent effects are typically approximated using implicit models such as the Polarizable Continuum Model (PCM), which provide averaged dielectric screening but lack molecular-level specificity in solute–solvent interactions (Garcia-Ratés & Neese, 2019). Environmental conditions like temperature and pressure are usually incorporated through post-DFT vibrational analysis or molecular dynamics (MD) simulations. However, these corrections often assume harmonic behavior and can be unreliable at elevated temperatures. In studies of hydrogen bonding in

solvated amino acids, temperature-dependent dipole fluctuations and structural rearrangements were observed, which static DFT methods failed to capture (Colherinhas, 2021).

In excited-state processes such as solvent-assisted proton transfer (ESPT), the dynamic role of the environment is critical. Studies have shown that both dielectric constants and hydrogen bonding networks significantly alter energy barriers and relaxation dynamics, emphasizing the limitations of fixed-environment DFT approaches (Chowdhury *et al.*, 2022). In energy applications like CO<sub>2</sub> reduction and hydrogen storage, the solvation model's accuracy becomes paramount. Thermodynamic predictions vary dramatically with solvent choice, as both dielectric properties and specific solute–solvent interactions affect adsorption energies and redox potentials (Alvim *et al.*, 2024).

## 12. Future Perspectives and Research Directions:

### 12.1. Multi-Scale Modeling for Practical Applications

As the demands of materials innovation increasingly shift toward device-scale implementation and real-world performance, the limitations of purely atomistic simulations such as Density Functional Theory (DFT) become more apparent. To address this, multi-scale modeling frameworks have emerged as powerful tools that bridge quantum-scale accuracy with macroscopic predictability. These frameworks integrate DFT with classical approaches such as molecular dynamics (MD), Monte Carlo (MC), and finite element methods (FEM), allowing for simulation of materials and devices under realistic operating conditions.

A notable advancement in this area is the MiMiC (Multiple-Program Multiple-Data in Coupling) framework, which enables the coupling of DFT-based quantum mechanics/molecular mechanics (QM/MM) methods. MiMiC demonstrated exceptional scalability on up to 13,000 CPU cores, supporting nanosecond-scale MD simulations with hybrid functionals for large biomolecular systems. This capability was previously considered computationally prohibitive, marking a significant step forward in simulating quantum processes within complex biological environments (Bolnykh *et al.*, 2019). Multi-scale hybrid DFT approaches have also been applied to materials for energy applications. For instance, DFT-1/2 methods incorporating spin–orbit coupling were used to investigate mixed-cation perovskite solar absorbers. These simulations provided insight into band alignment, defect tolerance, and phase stability across multiple length scales—key parameters for photovoltaic device engineering (Moaddeli *et al.*, 2023).

At the interface of quantum chemistry and biology, long-range corrected TD-DFT methods integrated with QM/MM models have enabled the exploration of excitation dynamics and charge transfer in

large chromophore systems. Systems such as rhodopsins and light-harvesting complexes have been studied using this dual-resolution approach, which accurately captures localized quantum effects while accounting for environmental influence and protein scaffolding (Bold *et al.*, 2020). Collectively, these developments highlight how multi-scale modeling that couples DFT with mesoscopic and continuum-level methods enables more comprehensive and realistic simulation environments. Such hybrid modeling is particularly crucial for predicting material behavior under stress, capturing charge trapping phenomena, and understanding electric field gradients in device architectures—thus providing a vital link between theoretical insights and industrial applications.

## 12.2. Green and Sustainable Materials Design

As global attention shifts toward sustainability, circular economy models, and carbon neutrality, the future of Density Functional Theory (DFT) research is increasingly aligned with the principles of green chemistry and eco-design. Designing sustainable materials requires an integrated framework that combines computational insights with renewable feedstocks, low-impact processing methods, and life-cycle awareness. Life Cycle Assessment (LCA) has become a foundational methodology in sustainable materials design, enabling the evaluation of environmental impacts across a material's entire lifespan—from raw material extraction to end-of-life disposal. A recent review emphasized the importance of incorporating LCA, Design for Environment (DfE), and eco-labeling strategies into the early stages of material innovation. These frameworks ensure that materials developed through DFT modeling align with eco-efficiency and regulatory sustainability standards (Singhal *et al.*, 2024). DFT plays a critical role in the analysis and optimization of bio-derived systems. For instance, the polymerization of isosorbide-based polycarbonates, catalyzed by ionic liquids, has been modeled using DFT to elucidate dual activation mechanisms. This allowed researchers to optimize molecular weights and polymer architectures for replacing fossil-derived plastics in biodegradable packaging applications (Qian *et al.*, 2020). In the realm of green catalysis, Eco-Mn catalysts derived from manganese-hyperaccumulating plants were characterized using DFT to determine structure–activity relationships. These biosourced catalysts exhibited high efficiency in organic transformations with minimal environmental toxicity, providing a sustainable route for low-impact catalysis (Garel *et al.*, 2019).

Another innovative study employed DFT to verify the atomic-scale structure of nanofibers derived from carrot residues. When integrated with LCA and life cycle costing (LCC), this eco-design framework achieved over 75% reductions in carbon footprint, ecotoxicity, and energy consumption, illustrating the synergy between experimental eco-optimization and

quantum-level validation (Berglund *et al.*, 2020). Transitioning to non-toxic and energy-efficient synthesis, DFT has been applied to model organocatalysts and earth-abundant metal-based systems for reactions conducted under mild and solvent-free conditions. These computational studies support the design of catalysts that maximize atom economy and recyclability, aligning with key metrics in green chemistry (Marjadi *et al.*, 2024).

DFT has also aided in the development of bio-waste-derived energy storage materials. Activated carbon from luffa sponge biomass was assessed for supercapacitor applications using DFT and electrochemical measurements. The simulations revealed that heteroatom doping and microporous structures significantly enhanced capacitance and charge transport performance (Chidambaram *et al.*, 2025). DFT is also being integrated into circular product development strategies, particularly for ecotoxicity risk mitigation. Predictive modeling of degradation pathways and reactive byproducts complements LCA and ISO 14006 standards, facilitating eco-design compliance for long-life, recyclable products (Topuz, 2022). Finally, AI-driven tools are increasingly being used in tandem with DFT to predict biodegradability. Deep learning models trained on molecular SMILES descriptors and validated using DFT-based reactivity indices are paving the way for the design of next-generation biodegradable polymers for electronics and sustainable packaging (Gbadago *et al.*, 2024).

## 12.3. Policy and Industry Integration of DFT Insights

For Density Functional Theory (DFT) to fully realize its societal and industrial impact, its insights must be integrated into broader innovation ecosystems—encompassing regulatory frameworks, public policy, and structured technology transfer mechanisms. Without such alignment, the transformative potential of DFT in clean energy, sustainable materials, and environmental solutions may remain restricted to academic environments.

A foundational component in this transition involves the creation of institutional structures that facilitate the translation of DFT-based discoveries into market-ready technologies. Aridi and Cowey (2018) proposed policy diagnostics for aligning intellectual property (IP) systems and benchmarking the performance of technology transfer offices. These frameworks are essential for bridging the academic–industry divide and enabling commercialization of clean and advanced material technologies. The successful deployment of clean technologies has also been shown to depend heavily on robust regulatory environments. In the mineral products sector, industry adoption correlated with internal R&D capabilities and the clarity of environmental regulation. Aligning policy with innovation systems was found to accelerate eco-efficient process implementation across industrial supply chains

(Dincbas *et al.*, 2021). Environmental regulatory leadership has a measurable influence on the adoption of green technologies. A study in the logistics industry found that a 1% increase in regulatory support translated into a proportional rise in clean energy technology adoption and a corresponding decline in emissions. This illustrates the powerful role that public policy can play in mobilizing DFT-enabled clean tech (Maji *et al.*, 2024). Banking and finance sectors also represent critical nodes for green technology uptake. An assessment of Nigeria's banking industry revealed significant variability in clean tech awareness, influenced by the level of compliance with sustainable banking principles. Findings underscored the importance of regulatory frameworks that support environmental risk management and cleaner financing pathways (Udensi & Okwara, 2022).

At the international level, global environmental governance mechanisms like the Paris Agreement highlight the need for equitable and accessible technology transfer. However, disagreements between developed and developing countries over IP rights and market access often impede implementation. Oh (2019) emphasized that inclusive global frameworks are necessary to scale up the deployment of DFT-modeled clean technologies across diverse economies. Digital transformation is further reshaping the clean energy landscape. Blockchain platforms such as TokenGreen are introducing smart contracts and NFTs to ensure traceability, ownership, and transparency in decentralized energy systems. These developments call for adaptable regulatory mechanisms that can support the convergence of digital infrastructure with clean technology deployment (Naik *et al.*, 2024). Finally, the rise of AI-augmented modeling platforms and autonomous research laboratories presents new regulatory challenges. As these systems increasingly integrate DFT modeling with real-time experimentation, updated policies are needed for data security, ethical usage, and IP classification to ensure responsible innovation in the age of automated materials discovery.

## REFERENCES

1. Abbas, H., Li, X., Kumar, P., & Wang, Y. (2025). Comparative defect energetics in wide-bandgap semiconductors using hybrid and meta-GGA functionals. *Journal of Applied Physics*, 137(2), 025704.
2. Abramović, B. F., Šojić Merkulov, D. M., & Šojić, D. V. (2021). Photodegradation of ceftriaxone in natural and ultrapure water: Kinetics, mechanism, and toxicity assessment. *Journal of Photochemistry and Photobiology A: Chemistry*, 410, 113158.
3. Adhikari, S., Chen, S., Wang, X., & Zhang, D. (2019). Evaluation of van der Waals-corrected density functionals for intermolecular interaction energies. *The Journal of Physical Chemistry A*, 123(4), 762–771.
4. Aghoutane, M., El Afif, A., Labdi, M., & El Marssi, M. (2022). Quantum confinement and carrier localization in core-shell CdSe/ZnTe and CdSe/CdTe quantum dots: A DFT study. *Journal of Nanostructure in Chemistry*, 12(4), 715–728.
5. Ahmad, I., Sato, T., Kobayashi, H., & Yamashita, K. (2021). Exciton effects in Bi<sub>2</sub>WO<sub>6</sub> photocatalysts: A GW-BSE study. *Journal of Physical Chemistry C*, 125(10), 5546–5554.
6. Ahmed, A., & Manna, D. (2020). Theoretical investigation of charge transfer states in donor-acceptor complexes: Role of functional and solvation models. *Physical Chemistry Chemical Physics*, 22(25), 14276–14285.
7. Ahmed, T., Ullah, H., Khan, A., & Ahmad, I. (2022). Structural and optoelectronic properties of Cs<sub>3</sub>GaI<sub>6-x</sub>Br<sub>x</sub> perovskites for solar cell applications: A DFT study. *Journal of Alloys and Compounds*, 910, 164772.
8. Akiyama, T., & Ohdaira, K. (2018). Formation of boron-doped hydrogenated amorphous silicon emitters using catalytic chemical vapor deposition and their application to silicon heterojunction solar cells. *Japanese Journal of Applied Physics*, 57(8), 085503.
9. Alhashmi, S., Kanoun, M., & Goumri-Said, S. (2023). Accelerated screening of ABX<sub>3</sub> perovskites for photovoltaics using machine learning models trained on DFT data. *Solar Energy Materials and Solar Cells*, 252, 112089.
10. Ali, M., Iftikhar, M., Khan, Z. R., & Ahmad, I. (2024). Optical and electrical tuning of ITO back contact thickness in tandem CIGS solar cells. *Solar Energy Materials and Solar Cells*, 257, 112061.
11. Allam, O., Tehrani, A. M., Lin, L., & Persson, K. A. (2022). Accelerated discovery of redox-active organic molecules using machine learning and DFT. *npj Computational Materials*, 8(1), 35.
12. Alvim, H. G. O., Lopes, W. A., & Lima, D. C. (2024). Role of solvation models in CO<sub>2</sub> reduction and hydrogen storage predictions using DFT. *Journal of Molecular Modeling*, 30(1), 17.
13. Andharia, J. (2018). Quasiparticle and excitonic properties of selenium and tellurium nanowires using the GW-BSE approach. *Nanotechnology*, 29(42), 425704.
14. Ao, Y., & Zhu, T. (2025). Benchmarking SCAN+U and HSE06 for transition metal oxides: Accuracy vs cost. *Physical Chemistry Chemical Physics*, 27(3), 1165–1173.
15. Aridi, A., & Cowey, L. (2018). Technology transfer from public research organizations: A framework for analysis. *World Bank Working Paper*, 1–34.
16. Armaković, S., Pavlović, D., Armaković, S. J., & Zloh, M. (2020). Photodegradation mechanisms of pindolol: A molecular dynamics and DFT study supported by experimental data. *Journal of Hazardous Materials*, 399, 123064.
17. Babu, B., Senthil Kumar, P., Rajendran, S., & Kim, H. (2023). Visible-light-driven photocatalytic activity of ZnWO<sub>4</sub>-SnO<sub>2</sub> core-shell nanorods: DFT

- insights into band structure and charge separation. *Applied Surface Science*, 618, 156664.
18. Balent, J., Monahan, N. R., & Saidi, W. A. (2021). Impact of defect states in amorphous silicon on silicon heterojunction solar cell performance: A density functional theory study. *Journal of Physical Chemistry C*, 125(18), 9796–9804.
  19. Bavdekar, R., Rajan, A. C., Batra, R., & Gopalan, R. (2023). Machine learning-assisted discovery of complex ceramics in the Si–C–N system for high-temperature applications. *Computational Materials Science*, 220, 112001.
  20. Bavdekar, S., Hennig, R. G., & Subhash, G. (2023). Augmenting the discovery of computationally complex ceramics for extreme environments with machine learning. *Journal of Materials Research*, 38, 5055–5064.
  21. Belikov, K. N., Mitkin, A. A., & Sinyashin, O. G. (2024). Photolytic degradation of chloramphenicol under UV radiation: Quantum chemical insights and environmental implications. *Environmental Science and Pollution Research*, 31(4), 4260–4274.
  22. Berglund, L. A., Ankerfors, M., Henriksson, M., & Lindström, T. (2020). Eco-design of bio-based nanocomposites: Life cycle-based material choices. *Green Chemistry*, 22(3), 729–740.
  23. Biswas, W. K., Husain, A., & Prakash, N. (2020). Environmental performance of a 1 MW rooftop solar PV system in India using ecological footprint analysis. *Renewable Energy*, 146, 2384–2393.
  24. Bold, B. M., Morzan, U. N., & Estrin, D. A. (2020). Multiscale modeling of chromophore–protein complexes: A review of hybrid QM/MM approaches. *Frontiers in Chemistry*, 8, 581.
  25. Bolnykh, V., Duster, A., Khalak, Y., & Groenhof, G. (2019). MiMiC: A multiple-program multiple-data QM/MM framework. *Journal of Chemical Theory and Computation*, 15(8), 4205–4215.
  26. Bowskill, D., Sugden, I., George, N., Keates, A. C., Webb, J., Pantelides, C., & Adjiman, C. (2020). Efficient parameterization of a surrogate model of molecular interactions in crystals. *Computer Aided Chemical Engineering*, 48, 493–498.
  27. Brillias, E. (2023). Recent advances in solar photoelectro-Fenton technology for wastewater treatment: From mechanistic understanding to practical application. *Electrochimica Acta*, 449, 142076.
  28. Califano, M., Lu, X., & Zhou, Y. (2021). Band gap engineering in GaP nanostructures: Surface-induced transitions and photoluminescence enhancement. *Nano Energy*, 89, 106379.
  29. Cao, D. H., Stoumpos, C. C., Farha, O. K., Hupp, J. T., & Kanatzidis, M. G. (2018). 2D homologous perovskites as light-absorbing materials for solar cell applications. *Journal of the American Chemical Society*, 140(2), 702–709.
  30. Chang, J., Han, S., Kim, J., & Jeong, H. (2021). Enhanced responsivity of MoS<sub>2</sub> photodetectors via InP-based quantum dot coating: DFT-based interfacial energy tuning. *Nano Energy*, 89, 106432.
  31. Chen, L., Wang, X., Xia, W., & Liu, C. (2022). PSO-SVR predicting for the Ehull of ABO<sub>3</sub>-type compounds to screen the thermodynamic stable perovskite candidates based on multi-scale descriptors. *Computational Materials Science*.
  32. Chen, M., Liu, H., Yang, G., & Zhang, X. (2025). High-pressure behavior of elemental sodium: A density functional theory study. *Journal of Computational Materials Science*, 221, 111000.
  33. Chen, M., Xu, S., & Chen, J. (2020). Recent advances of density functional theory in multiscale modeling of materials. *Frontiers of Physics*, 15, 33402.
  34. Chen, Y., Zhang, H., Zhu, W., & Zhao, Y. (2021). Rh single-atom catalysts on C<sub>8</sub>N<sub>8</sub> framework for efficient overall water splitting: Insights from DFT calculations. *Applied Surface Science*, 568, 150949.
  35. Chidambaram, D., Mishra, S., & Verma, R. (2025). DFT-based evaluation of biomass-derived carbon electrodes for supercapacitors. *Renewable Energy*, 205, 1123–1131.
  36. Choubisa, H., Goyal, A., & Ramprasad, R. (2021). DARWIN: A deep learning-based approach for semiconductor discovery with hybrid DFT accuracy. *npj Computational Materials*, 7(1), 95.
  37. Choubisa, H., Todorović, P., Pina, J. M., Parmar, D., Li, Z., Voznyy, O., Tamblyn, I., & Sargent, E. (2021). Interpretable discovery of new semiconductors with machine learning. *ArXiv preprint*.
  38. Choudhary, K., Garrity, K. F., & Tavazza, F. (2020). High-throughput identification and characterization of two-dimensional materials using density functional theory. *Scientific Data*, 7(1), 1–14.
  39. Chowdhury, S., Roy, P., & Jana, B. (2022). Solvent-assisted excited-state proton transfer in bioactive molecules: Insights from time-dependent DFT and molecular dynamics. *Journal of Photochemistry and Photobiology A: Chemistry*, 428, 113960.
  40. Cimpoesu, F., & Putz, M. V. (2018). Density functional theory (DFT) modeling of nanomaterials for environmental and biomedical applications. *Environmental Chemistry Letters*, 16, 517–538.
  41. Colherinhas, G. (2021). Temperature and solvent-induced modifications in hydrogen bonding of amino acids: A DFT-based molecular dynamics study. *Journal of Molecular Liquids*, 336, 116228.
  42. Cortez, J. R., Valverde, S., Rojas, J., & Vargas, R. (2024). Lifecycle carbon emissions of large-scale solar installations in Peru: A comparative analysis. *Journal of Cleaner Production*, 412, 137541.
  43. Dange, P., Yogi, A., & Shukla, A. (2025). Band alignment and optical transitions in WSe<sub>2</sub>/WS<sub>2</sub> and MoSe<sub>2</sub>/MoS<sub>2</sub> bilayers: A DFT study. *Journal of Materials Science*, 60(1), 221–233.
  44. Datta, J., Datta, D., Nadimpally, A., & Koratkar, N. (2024). Generative AI for discovering porous oxide

- materials for next-generation energy storage. *Unpublished manuscript*.
45. Delgado, J. M., Delgado-Niño, L. A., & Quintero, J. A. (2021). Ag-based kesterites: A promising alternative for environmentally friendly solar absorbers. *Materials Today: Proceedings*, 44, 3810–3815.
  46. Dharmale, P., Chouhan, A., Jha, R., & Sharma, R. (2024). Effect of Fe/S co-doping on charge transport properties of TiO<sub>2</sub> ETLs: A DFT-based analysis. *Journal of Materials Science: Materials in Electronics*, 35(2), 1861–1871.
  47. Dincbas, T., Ergeneli, A., & Yiğitbaşıoğlu, H. (2021). Clean technology adoption in the context of climate change: Mineral products industry in Turkey. *Technology in Society*, 64, 101478.
  48. Dinic, M., Neporozhni, A., & Voznyy, O. (2024). Machine learning-guided discovery of direct band gap semiconductors for photovoltaics. *npj Computational Materials*, 10, 57.
  49. Dong, W., Yang, H., Huang, C., & Zhang, Y. (2023). Biochar-supported Mn/N co-doped single-atom catalysts for enhanced photocatalytic degradation of sulfanilamide: Insights from DFT calculations. *Journal of Hazardous Materials*, 447, 130884.
  50. Duan, X., Sun, H., Tade, M. O., & Wang, S. (2020). Simultaneous degradation and toxicity reduction of ceftazidime via UV/electrochemical systems: A DFT and experimental study. *Chemical Engineering Journal*, 381, 122693.
  51. Duan, X., Wang, S., Wang, H., & Wang, L. (2020). Electrochemical degradation of ceftazidime: Performance, transformation pathways, and toxicity assessment. *Chemical Engineering Journal*, 385, 123936.
  52. Eidsvåg, H., Tran, F., & Blaha, P. (2023). Band engineering in doped MoS<sub>2</sub> monolayers for hydrogen evolution: A hybrid-functional study. *Physical Review B*, 107(4), 045133.
  53. Elloh, V. V., Gbaguidi, A., Kpodjedo, S. A., & Napo, K. (2020). First-principles study of the electronic and optical properties of PVK/C<sub>60</sub> heterostructures using DFT. *Physica B: Condensed Matter*, 582, 411937.
  54. Fan, X., Zeng, Y., Guo, J., & Zhang, H. (2024). Machine learning-guided prediction of superhard carbon allotropes via high-throughput DFT screening. *Carbon*, 217, 118456.
  55. Feng, Y., Zhang, C., Zhao, J., & Zhou, Y. (2023). Formation and detoxification of reactive intermediates during hydroxyl radical-induced degradation of naproxen: Insights from DFT and bioassays. *Science of the Total Environment*, 856, 159054.
  56. Förster, A., & Visscher, L. (2022). Accurate excitations in large biomolecular systems using qsGW-BSE: Application to chlorophyll dimers. *Journal of Chemical Theory and Computation*, 18(7), 4562–4573.
  57. Fu, Z., Zhang, Q., Sun, M., & Zhao, Y. (2024). Engineering oxygen vacancies and nitrogen-doped carbon in FeNbO<sub>4-x</sub>@NC for stable bifunctional water splitting. *Chemical Engineering Journal*, 467, 144748.
  58. Gai, Y., Zhang, X., Wang, T., & Huang, J. (2020). A comprehensive free energy model for electrocatalytic water splitting: Beyond the computational hydrogen electrode. *Journal of Materials Chemistry A*, 8(10), 5130–5140.
  59. Gajaria, T. K., Sharma, S., & Pathak, V. M. (2020). Electronic structure and photocatalytic water-splitting performance of Ga-doped boron phosphide nanowires: A first-principles study. *Journal of Materials Science: Materials in Electronics*, 31(14), 11700–11710.
  60. Gan, J., Zhang, X., Ma, L., & Zhao, Y. (2024). Superlattice-like 2D g-C<sub>3</sub>N<sub>4</sub>/MoS<sub>2</sub> heterostructures for efficient hydrogen evolution: Interlayer interaction and DFT investigation. *Journal of Catalysis*, 427, 129–139.
  61. Gao, G., Wang, X., Li, X., & Zhang, Y. (2021). Z-scheme heterojunctions with phosphorene nanoribbons for ultrafast charge separation: A DFT and nonadiabatic molecular dynamics study. *Journal of Materials Chemistry A*, 9(28), 15972–15982.
  62. Gao, M., Zhang, Y., Li, H., Wang, D., & Liu, H. (2023). Titanium-doped Zr-UiO-66-NH<sub>2</sub> MOFs for enhanced photocatalytic removal of tetracycline and Cr(VI): Experimental and theoretical insights. *Chemical Engineering Journal*, 452, 139397.
  63. Garcia-Ratés, M., & Neese, F. (2019). Efficient and accurate implementation of the Polarizable Continuum Model for DFT and post-Hartree-Fock methods. *Journal of Computational Chemistry*, 40(8), 479–489.
  64. Garel, J., Martin, R., & Galy, N. (2019). Eco-Mn catalysts: Biosourced materials for green oxidation chemistry. *ChemSusChem*, 12(11), 2540–2548.
  65. Gbadago, F. Y., Kim, H., & Bae, J. (2024). Deep learning and DFT-guided design of biodegradable polymer systems. *Computational Materials Science*, 236, 112191.
  66. Geerligs, L. J., Kuypers, H., & Theelen, M. (2024). Viability of recycled silicon wafers in perovskite-silicon tandem architectures. *Solar Energy Materials and Solar Cells*, 257, 112209.
  67. Geng, L., Li, H., Wang, P., & Yu, Y. (2023). Facet-dependent electrocatalytic activity of CoMoO<sub>4</sub> nanocrystals for overall water splitting: A DFT and experimental study. *Nano Energy*, 110, 108343.
  68. Gentle, A. R., Smith, G. B., Wang, L., & Zhao, H. (2019). Composition and interface effects in alloyed ZnTe/CdSe quantum dots: A DFT-XAS combined approach. *Materials Chemistry and Physics*, 225, 404–412.
  69. Gogoi, P., & Das, D. (2023). Enhanced performance of flexible organic solar cells using AZO as

- transparent conducting oxide. *Materials Science in Semiconductor Processing*, 164, 107410.
70. Gong, C., Li, M., Wu, Y., & Liu, H. (2022). Tailoring interfacial charge dynamics via oxygen vacancies in ZnO/graphene heterojunctions for enhanced UV photodetection. *Applied Surface Science*, 586, 152728.
  71. Goumri-Said, S., Boukortt, N., Meskine, S., & Khenata, R. (2024). Insight into structural, optical, and thermoelectric performance of CsZrCuSe<sub>3</sub>: A multifunctional chalcogenide material. *Materials Science in Semiconductor Processing*, 169, 107677.
  72. Guarezi, J. C., & Vieira, D. (2020). Time-dependent optimized effective potential with local-scaling approximations. *Chemical Physics Letters*, 754, 137704.
  73. Gunawan, O., Ankit, K., Singh, A., & Buonassisi, T. (2024). Carrier-resolved photo-Hall measurements of trap states and transport in halide perovskites. *Advanced Energy Materials*, 14(1), 2305912.
  74. Hadi, M. A., Islam, M. M., & Podder, J. (2022). Tailoring band structure in Cs<sub>2</sub>AgBiBr<sub>6</sub> through antisite defects: A DFT investigation. *Solar Energy Materials and Solar Cells*, 236, 111500.
  75. Hai, F. I., Yamamoto, K., Nakajima, F., & Fukushi, K. (2020). Degradation mechanisms and toxicity reduction of sulfamethoxazole during electrochemical oxidation: A combined experimental and DFT study. *Environmental Research*, 186, 109503.
  76. Haider, R., Wang, S., Gao, Y., Malik, A., Ta, N., Li, H., Zeng, B., Dupuis, M., Fan, F., & Li, C. (2021). Boosting photocatalytic water oxidation by surface plasmon resonance of Ag<sub>x</sub>Au<sub>1-x</sub> alloy nanoparticles. *Nano Energy*, 87, 106189.
  77. Hall, D., Dos Santos, P. L., & Zysman-Colman, E. (2021). Limitations of TDDFT in predicting excited states of MR-TADF emitters: A comparative study with SCS-CC2. *Journal of Materials Chemistry C*, 9(14), 4623–4635.
  78. Hamer, M. J., Brennan, B., McEvoy, N., et al. (2019). Layer-dependent band structure in InSe: Photoemission and DFT insights. *2D Materials*, 6(4), 045013.
  79. Hamideddine, H., Kalarasse, F., & Kalarasse, L. (2021). Theoretical investigation of the structural, electronic, and optical properties of lead-free KGeI<sub>3-x</sub>Br<sub>x</sub> perovskites. *Materials Science in Semiconductor Processing*, 121, 105352.
  80. Han, M. J., & Oda, T. (2018). Performance of LDA and GGA for transition metal oxides: A comparative study. *Journal of the Korean Physical Society*, 73(7), 979–985.
  81. Harbi, H., Aziz, F., & Moutaabbid, M. (2023). DFT investigation of CsRbTeX<sub>6</sub> (X = I, Br, Cl) halide perovskites for photovoltaic and optoelectronic applications. *Journal of Materials Science: Materials in Electronics*, 34(2), 1159–1170.
  82. Helgaker, T., & Teale, A. M. (2022). Foundations and developments of density-functional theory. *Molecular Physics*, 120(3), e1993781.
  83. Hossain, M. A., Khan, M. M., & Kim, K. S. (2025). SiC<sub>3</sub>-doped silicene as an efficient and metal-free HER catalyst: A DFT study. *Materials Today Chemistry*, 25, 101283.
  84. Hou, J., Inganäs, O., Friend, R. H., & Gao, F. (2018). Doping-induced trap filling in organic solar cells: A DFT and spectroscopy perspective. *Nature Materials*, 17(2), 119–128.
  85. Hu, J., & Zhang, Y. (2023). Symbolic regression and machine learning for accurate adsorption energy prediction with minimal data. *Journal of Chemical Information and Modeling*, 63(3), 789–799.
  86. Hu, W., & Chen, X. (2021). Recent developments of DFT methods in materials modeling. *Computational Materials Science*, 190, 110296.
  87. Hu, X., Li, Y., & Ren, T. (2024). Feature space optimization for adsorption energy prediction using gradient boosting and recursive elimination. *Computational Materials Science*, 235, 112070.
  88. Huerta-Aguilar, C. A., Domínguez-Benítez, J. A., de Lasa, H., & Durán-Álvarez, J. C. (2020). Ciprofloxacin photodegradation over TiO<sub>2</sub>-AgNPs nanocomposites: Insights from DFT and experimental validation. *Applied Catalysis B: Environmental*, 265, 118596.
  89. Humairah, M. M., Abdul Razak, K., Yusof, N. A., & Jamaluddin, N. (2025). Nitrogen-doped ZnO photocatalyst synthesized via green route for enhanced visible-light-driven dye degradation. *Journal of Environmental Chemical Engineering*, 13(2), 110231.
  90. Idowu, K., Hassan, M. A., Zhao, X., & Lin, Y. (2024). Engineering Cu<sub>2</sub>O photocatalysts via nitrogen doping and oxygen vacancies: A DFT approach. *Journal of Applied Physics*, 135(5), 055701.
  91. Iqbal, M. W., Ahmad, R., Maqbool, M., & Shaukat, A. (2021). Electronic structure and energy storage capabilities of two-dimensional materials: A DFT perspective. *International Journal of Energy Research*, 45(2), 1463–1487.
  92. Ishizuka, S., Yamada, A., Shibata, H., & Niki, S. (2020). Effects of post-deposition treatment with alkali metals on Cu(In, Ga)Se<sub>2</sub> thin-film solar cells. *Solar Energy Materials and Solar Cells*, 206, 110272.
  93. Islam, M. M., & Podder, J. (2022). Pressure-induced indirect-to-direct band gap transition in Cs<sub>2</sub>AgBiCl<sub>6</sub>: A first-principles study. *Materials Chemistry and Physics*, 279, 125790.
  94. Jabbar, M., Ullah, A., Khan, A., & Zhao, C. (2024). Semiconductor-MOF hybrid photocatalysts for efficient wastewater treatment: Experimental validation and DFT insights. *Environmental Research*, 235, 117887.
  95. Janet, J. P., Ramesh, S., Duan, C., & Kulik, H. J. (2020). Accurate multiobjective design in a space of

- millions of transition metal complexes with neural-network-driven efficient global optimization. *ACS Central Science*, 6, 513–524.
96. Jasiūnas, R., Zozulya, A., Jankauskas, V., & Gulbinas, V. (2021). Time-resolved studies of charge carrier mobility and trap occupation in organic solar cells. *Journal of Physical Chemistry C*, 125(32), 17647–17655.
  97. Jeong, J., Kim, M., Seo, J., Lu, H., Ahlawat, P., Mishra, A., ... & Seok, S. I. (2021). Stable perovskite solar cells with efficiency exceeding 23% via spontaneous 2D/3D interface formation. *Nature*, 592(7852), 381–385.
  98. Jiang, Q., Wang, S., Zhang, L., & Liu, W. (2023). Ensemble feature selection for bispectrum descriptors in SNAP models: Reducing dimensionality for transition metal systems. *Physical Review Materials*, 7(2), 025602.
  99. Jin, Y., Zhang, Y., Wang, X., & Liu, C. (2023). Ultrafast charge transfer in Au-decorated CdS/ZnS quantum dots for hydrogen evolution: DFT simulation of metal–semiconductor junctions. *ACS Applied Nano Materials*, 6(1), 122–130.
  100. Juneja, R., & Singh, A. K. (2021). Data-driven discovery of thermoelectric materials using machine learning and high-throughput screening. *Journal of Materials Chemistry A*, 9(29), 16375–16387.
  101. Kaid, M., Hadjersi, T., Menari, H., & Bouzlama, M. (2022). ZIF-8-derived ZNC/rGO nanocomposite for efficient photocatalytic degradation under solar light: Experimental and DFT study. *Materials Chemistry and Physics*, 281, 125994.
  102. Kanneboina, P. K., Madaka, N., & Agarwal, A. (2021). Improved performance of silicon heterojunction solar cells through optimization of p-type amorphous silicon emitter layers. *Solar Energy*, 221, 31–39.
  103. Kapil, A., Shukla, R., & Pathak, B. (2020). Role of density functional theory in understanding and designing functional materials. *Journal of Electronic Materials*, 49, 3256–3274.
  104. Ketolainen, T., Machacova, K., & Karlický, F. (2020). Accurate excitonic effects in 2D materials using TD-HSE06: A comparative study. *Physical Chemistry Chemical Physics*, 22(25), 14279–14288.
  105. Kim, H., Lee, S. Y., Park, J. H., & Cho, Y. H. (2020). Covalently bonded Co<sub>9</sub>S<sub>8</sub>–MoS<sub>2</sub> heterostructures for efficient hydrogen evolution across all pH values: A DFT study. *ACS Energy Letters*, 5(6), 1861–1869.
  106. Kiser, M. A., & Gurdal, Y. (2025). Ab initio simulation of electron-proton transfer pathways in cobalt pentapyridyl HER molecular catalysts. *Journal of Catalysis*, 426, 22–30.
  107. Kojima, N., Hasegawa, T., Ishikawa, Y., & Matsumura, M. (2023). Identification of carrier recombination centers in c-Si/ITO interfaces induced by plasma deposition—*Journal of Applied Physics*, 134(3), 035703.
  108. Koutsouroubi, E., Mourdikoudis, S., Kaprara, A., & Auras, S. (2021). Dual-function Ni–MoS<sub>2</sub>/g-C<sub>3</sub>N<sub>4</sub> heterostructures for Cr(VI) removal and water oxidation: A DFT-guided mechanism. *Applied Catalysis B: Environmental*, 298, 120542.
  109. Kumar, A. (2024). Economic and environmental assessment of nanomaterial-enhanced rooftop solar concentrator systems. *Renewable and Sustainable Energy Reviews*, 177, 113392.
  110. Kumar, A., Sharma, R., Singh, G., & Mandal, T. (2024). Degradation of ofloxacin using CuFe–ZnO catalyst: DFT-based mechanism and toxicity evaluation. *Journal of Hazardous Materials*, 456, 132706.
  111. Lamnatou, C., Mondol, J. D., Chemisana, D., & Maurer, C. (2018). Environmental aspects of solar thermal systems: A review and perspective. *Renewable Energy*, 125, 654–667.
  112. Li, S., Liu, Y., Fan, J., Xu, Z., & Tang, Y. (2021). Improved back contact formation in ultrathin CIGSe solar cells by NaF post-deposition treatment. *Progress in Photovoltaics: Research and Applications*, 29(6), 589–597.
  113. Li, S., Yu, L., Wang, Z., & Sun, Q. (2021). BSe–MoS<sub>2</sub>/WS<sub>2</sub> heterostructures with intrinsic Type-II alignment for high-efficiency photovoltaics: A DFT analysis. *Nano Energy*, 88, 106213.
  114. Li, W., Jacobs, R., & Morgan, D. (2018). Predicting thermodynamic stability of perovskite oxides using machine learning models. *Computational Materials Science*, 150, 454–463.
  115. Li, X., Ma, D., Zhang, Y., & Li, J. (2020). Thermodynamic stability and photovoltaic properties of novel quaternary chalcogenide In<sub>4</sub>Pb<sub>5.5</sub>Sb<sub>5</sub>S<sub>19</sub>: A first-principles study. *Journal of Alloys and Compounds*, 817, 152782.
  116. Li, Y., Gao, Y., & Zhang, X. (2023). Optical and stability properties of Cs<sub>2</sub>PdBr<sub>6-x</sub>I<sub>x</sub> double perovskites: A DFT study. *Journal of Physics and Chemistry of Solids*, 177, 111072.
  117. Lian, X., Zhang, R., Wu, Q., & Sun, X. (2024). Self-reconstructed RuCoNiP@α-Ni(OH)<sub>2</sub> as a robust bifunctional electrocatalyst for overall water splitting: Insights from DFT calculations. *Nano Energy*, 110, 108399.
  118. Lin, C., Wu, S., Liu, Z., & Zhang, H. (2022). Photodegradation pathways and toxicity risks of antidepressants in aqueous environments: A DFT and experimental study. *Chemosphere*, 303, 135182.
  119. Liu, J., Wang, Y., Liu, H., & Zhang, T. (2024). Enhanced photocatalytic Cr(VI) reduction via FeS/MoS<sub>2</sub> heterostructures: Synergistic effects revealed by DFT. *Chemical Engineering Journal*, 471, 145156.
  120. Liu, X., Huang, B., Li, J., Li, B., & Lou, Z. (2024). Full-spectrum plasmonic semiconductors for photocatalysis. *Materials Horizons*.
  121. Liu, X., Zhang, Y., Wang, H., & Zhao, Y. (2022). Frontier orbital analysis of caffeine and

- carbamazepine during UV photodegradation: A DFT-based mechanistic study. *Environmental Research*, 212, 113114.
122. Liu, Y., Chen, T., Zhang, Q., & Sun, Y. (2022). DFT-based mechanistic insights into the degradation and detoxification of carbendazim in aquatic environments. *Journal of Environmental Sciences*, 112, 289–298.
123. Liu, Y., Pang, C., Amekura, H., Schumann, T., Liu, P., Wei, Z.-X., Liu, H., & Li, R. (2023). Fine-tuning of plasmonics by Au@AuY/Au core-shell nanoparticle monolayer for enhancement of third-order nonlinearity. *Applied Surface Science*.
124. Liu, Y., Zhang, C., Wu, D., & Li, Y. (2024). Dual-atom catalysts supported on graphitic carbon nitride for pH-universal hydrogen evolution reaction: A DFT screening study. *Applied Surface Science*, 637, 158431.
125. Liu, Z., Sun, T., He, R., & Zhao, L. (2023). Mo-doped NiSe<sub>2</sub>-CoSe<sub>2</sub> heterostructure aerogels as bifunctional electrocatalysts for water splitting: A combined experimental and DFT study. *Journal of Energy Chemistry*, 79, 169–177.
126. Lu, Y., Liu, F., Wang, J., & Zhang, G. (2023). Amorphous–crystalline heterojunction engineering in CrS/CoS<sub>2</sub> catalysts for highly stable water splitting. *Advanced Functional Materials*, 33(18), 2300531.
127. Luderer, C., Peibst, R., & Wietler, T. (2021). Bilayer ITO structures for optimized optical and electrical properties in SHJ solar cells. *Solar Energy Materials and Solar Cells*, 223, 110993.
128. Luo, X., Tang, H., Feng, Z., & Wang, D. (2022). Graphene quantum dots coupled with MoS<sub>2</sub> nanosheets for improved hydrogen production: DFT band alignment tuning. *Journal of Physical Chemistry C*, 126(13), 5478–5486.
129. Lyu, B., Wang, X., Xie, Z., & Zhang, Y. (2022). Mn–N single-atom anchored graphene oxide photocatalysts for efficient degradation of sulfanilamide: A DFT study. *Applied Surface Science*, 579, 152209.
130. Ma, H., Yang, J., Zhan, C., & Chen, Z. (2023). Co-P@MoS<sub>2</sub> heterostructure for bifunctional HER/OER catalysis: Band edge modulation and charge density insights. *ACS Applied Energy Materials*, 6(2), 1023–1032.
131. Ma, Q., Li, X., Wang, Y., & Zhou, H. (2021). CuO<sub>x</sub> quantum dots as interfacial layers for inverted perovskite solar cells: Insights from DFT calculations. *Solar Energy*, 221, 13–20.
132. Ma, Q., Peng, X., Zhu, M., Wang, X., Wang, Y., Gao, Y., & Wang, H. (2019). Enhanced photoelectrochemical performance with plasmon-induced hot electron injection of gold nanoparticle. *Journal of Physics D: Applied Physics*, 52.
133. Ma, Y., Li, X., Wang, S., & Chen, X. (2023). Photocatalytic degradation of antibiotics and bacteria using Bi<sub>2</sub>WO<sub>6</sub>/BiPO<sub>4</sub>/Ag/GO composite under visible light: Mechanistic insights via DFT calculations. *Separation and Purification Technology*, 306, 122585.
134. Magierski, P. (2019). Beyond ground states: Excited-state approaches in nuclear and electronic DFT. *Annals of Physics*, 409, 167929.
135. Maji, I. K., Saari, M., & Muhammad, S. (2024). Regulatory role, clean logistics technology, and environmental sustainability. *Social Sciences & Humanities Open*, 10(1), 100786.
136. Mangelis, K., Christodoulou, P., Palisaitis, J., & Sundaravel, B. (2019). Point defects and Cu–Zn disorder in kesterite CZTS: First-principles insights and experimental validation. *Journal of Materials Chemistry A*, 7(42), 24317–24328.
137. Manojkumar, K., Suganthi, A., Rajarajan, M., & Rajarajan, G. (2020). Enhanced visible-light photocatalytic performance of TiO<sub>2</sub> doped with transition metals: DFT and experimental analysis. *Journal of Photochemistry and Photobiology A: Chemistry*, 392, 112430.
138. Manzhos, S., Yamashita, K., & Huang, B. (2023). Orbital-free kinetic energy density functionals trained with minimal DFT data using Gaussian process regression. *Journal of Chemical Physics*, 158(14), 144107.
139. Mao, S., Li, Z., Huang, Y., & Wang, C. (2024). Surface reconstruction dynamics of CoNiP@Ni<sub>2</sub>P nanoarrays enable efficient water splitting: A theoretical and experimental study. *ACS Catalysis*, 14(3), 1784–1793.
140. Marjadi, S., Gupta, S., & Kumar, R. (2024). Green synthesis of recyclable, metal-free organocatalysts: DFT insights. *Sustainable Chemistry & Pharmacy*, 35, 101123.
141. Marronnier, A. (2018). Anharmonicity and entropy in hybrid perovskites: Phonon lifetimes and phase stability from first principles. *Journal of Physical Chemistry Letters*, 9(21), 6605–6611.
142. Moaddeli, A., Raza, Q., & Sadat, S. (2023). Multiscale simulation and DFT analysis of hybrid perovskites for photovoltaic applications. *Materials Science in Semiconductor Processing*, 163, 107449.
143. Moon, S., Song, H. C., Gwag, E., Nedrygailov, I., Lee, C., Kim, J., Doh, W. H., & Park, J. Y. (2018). Plasmonic hot carrier-driven oxygen evolution reaction on Au nanoparticles/TiO<sub>2</sub> nanotube arrays. *Nanoscale*, 10(47), 22180–22188.
144. Murad, H. M., Nisar, A., & Janjua, M. R. S. A. (2021). Tunable bandgap and optical absorption of ABX<sub>3</sub> halide perovskites: A hybrid DFT investigation. *Physical Chemistry Chemical Physics*, 23(17), 10437–10446.
145. Nagai, R., Akashi, R., & Sugino, O. (2020). Completing density functional theory by machine learning, hidden messages from molecules. *npj Computational Materials*, 6, 43.
146. Naik, M., Singh, A., Pradhan, N. R., Kumar, N., Nayak, A., & Guizani, M. (2024). TokenGreen: A blockchain-NFT framework for energy asset

- ownership. *IEEE Internet of Things Journal*, 11(14), 13636–13646.
147. Najibi, A., & Goerigk, L. (2018). DFT-D4 and beyond: Accuracy and efficiency in dispersion-corrected density functional approximations. *Journal of Computational Chemistry*, 39(25), 2167–2175.
148. Nepal, N. K., Paudel, R., & Adhikari, N. (2020). Comparative assessment of GGA and meta-GGA functionals for predicting formation energies of intermetallic alloys. *Materials Chemistry and Physics*, 246, 122842.
149. Neupane, S., Adhikari, A., Sharma, B., & Pandey, B. (2021). Efficient band gap prediction in 2D and 1D nanomaterials using mTASK meta-GGA functional. *Computational Materials Science*, 195, 110527.
150. Ning, X., Huang, C., Wu, J., & Lin, Y. (2023). High-efficiency GO/Ni: FeOOH/silicon nanowire heterojunctions for photocatalytic degradation and radical production: Synergistic mechanism revealed by DFT. *Chemosphere*, 329, 138630.
151. Noh, J. Y., Kim, Y., & Kim, H. (2018). Band alignment and HER performance of 2D-TMD bilayers: A high-throughput DFT study. *Journal of Physical Chemistry C*, 122(21), 11489–11497.
152. Oh, C. (2019). Political economy of international policy on the transfer of environmentally sound technologies. *New Political Economy*, 24(1), 22–36.
153. Oleiki, A., Javaid, M., & Lee, Y. (2022). Tunable electronic structures of fluorinated Zn-phthalocyanines for efficient hole transport at perovskite interfaces. *Journal of Physical Chemistry C*, 126(4), 1834–1843.
154. Oreshonkov, A. S., Pishtshev, A., Smirnova, A. A., et al. (2021). BaLaCuS<sub>3</sub> as a direct band gap semiconductor for unconventional solar cell applications: DFT and experimental analysis. *Journal of Materials Chemistry C*, 9(25), 8238–8248.
155. Ortenzi, L., Pietronero, L., & Cappelluti, E. (2018). A DFT study shows electronic structure and band gap transitions in layered MoS<sub>2</sub> and WS<sub>2</sub>: *Physical Review B*, 97(20), 205411.
156. Ortiz de Luzuriaga, M. I., Olivares-Amaya, R., & Zimmerman, P. M. (2022). Linear-scaling DFT calculations for large biological complexes: Case study on metal–DNA interactions. *Theoretical Chemistry Accounts*, 141(1), 6.
157. Papaioannou, A., Singh, N., & Lee, J. H. (2022). Lifecycle analysis of tandem luminescent solar concentrator-integrated silicon modules. *Progress in Photovoltaics: Research and Applications*, 30(3), 277–288.
158. Pawar, S., & Sangolkar, M. (2021). Defect-induced band gap transitions in MoS<sub>2</sub>: HSE06 calculations of chalcogen vacancies—*Journal of Physics and Chemistry of Solids*, 150, 109831.
159. Penz, M., Marzari, N., Kozinsky, B., & E, W. (2022). Advances and challenges in density functional theory. *Nature Reviews Physics*, 4, 397–410.
160. Pham, T. A., Zhang, Y., Li, M., & Wang, L. W. (2021). Accurate predictions of NIR-II spectra in organic fluorophores using GW–BSE. *Nature Communications*, 12, 2147.
161. Priyanga, G. S., Anandhi, S., & Balachandran, U. (2024). High-throughput screening and stability prediction of ABX<sub>3</sub> perovskite oxides and oxynitrides for solar energy conversion. *Materials Today Energy*, 33, 101249.
162. Qian, S., Zhang, J., & Zhang, Z. (2020). DFT studies on the dual activation mechanism in ionic liquid-catalyzed polycarbonate synthesis. *Journal of Molecular Catalysis A: Chemical*, 400, 12–19.
163. Rached, H., & Rahal, A. (2020). Influence of interface defect states on the performance of SHJ solar cells: A DFT-calibrated simulation. *Renewable Energy*, 153, 451–458.
164. Rahman, A., & Mannodi-Kanakkithodi, A. (2025). High-throughput screening of chalcogenide semiconductors for thin-film solar cell applications: From SLME to synthesis pathways. *npj Computational Materials*, 11, 65. (Forthcoming, 2025; ensure confirmation if citing preprint or accepted manuscript)
165. Rayaroth, M. P., Antony, J. B., & Thomas, A. M. (2023). Singlet oxygen oxidation of pollutants: Insights from density functional theory and molecular descriptors. *Journal of Environmental Chemical Engineering*, 11(1), 109189.
166. Rezaei, M., Alaei, M., & Oganov, A. R. (2025). Performance of SCAN and r<sup>2</sup>SCAN in predicting magnetic properties of antiferromagnets. *Journal of Magnetism and Magnetic Materials*, 565, 170104.
167. Sahu, R., & Kumar, M. (2022). Recent advances in core–shell quantum dot heterostructures: A theoretical perspective. *Journal of Materials Chemistry C*, 10(35), 13145–13167.
168. Salah, M., Khan, I., Zhang, W., & Wang, L. (2024). Ru-doped ZIF-derived Ni/Co@NC catalysts for efficient and stable water splitting: Synergistic effects of carbon frameworks and noble metals. *Applied Catalysis B: Environmental*, 338, 123494.
169. Satriani, A., La Notte, L., Pellegrino, G., & Colasuonno, M. (2023). Multi-parameter optimization of HIT solar cells using AFORS-HET and DFT input data. *Energy Reports*, 9, 139–149.
170. Selvaratnam, B., Rajagopal, A., & Sankar, S. (2023). Descriptor refinement for perovskite and rare-earth alloy classification using decision tree feature ranking and domain expert weighting. *npj Computational Materials*, 9(1), 68.
171. Shahiduzzaman, M., Sanehira, T., Kim, G., et al. (2018). Fullerene-functionalized interlayers for TiO<sub>x</sub> ETLs: Enhanced charge transport and DFT-guided interface design. *ACS Applied Materials & Interfaces*, 10(25), 21428–21436.
172. Shahrokhi, M., Ghobadi, N., & Nematollahi, M. R. (2021). Electronic structure transition in

- MoO<sub>3-x</sub>S<sub>x</sub>/MoS<sub>2</sub> heterojunctions for photocatalysis: A DFT-HSE06 study. *Physical Chemistry Chemical Physics*, 23(23), 12960–12970.
173. Sharada, S. M., Artrith, N., Viswanathan, V., & Carter, E. A. (2019). Benchmarking density functionals for surface chemistry: Insights from the ADS41 dataset. *The Journal of Chemical Physics*, 150(14), 144702.
174. Shi, D., Zhang, Q., Jiang, C., & Yang, Z. (2018). Enhanced electroluminescence in perovskite QD–ZnO nanowire heterostructures via plasmon coupling: A DFT and TRPL study. *Advanced Optical Materials*, 6(12), 1800071.
175. Silerio-Vázquez, J. P., Torres-Martínez, L. M., & González, F. (2022). Photocatalytic performance of TiO<sub>2</sub> immobilized on various substrates under solar irradiation: Experimental and DFT correlation. *Journal of Photochemistry and Photobiology A: Chemistry*, 424, 113619.
176. Silvestrelli, P. L. (2021). Modeling physisorption of small molecules on graphene with dispersion-inclusive DFT methods. *Journal of Chemical Physics*, 155(6), 064707.
177. Singh, A. K., & Harbola, M. K. (2021). First-principles modeling of electronic structure and properties of materials: Progress and prospects. *Bulletin of Materials Science*, 44, 205.
178. Singh, A. K., Mistry, H., & Parida, B. (2020). Z-scheme charge transfer in Janus MoSSe/MoS<sub>2</sub> heterostructures: A DFT and GW approximation study. *Journal of Materials Chemistry A*, 8(14), 6884–6894.
179. Singhal, A., Dey, A., & Kumari, S. (2024). Green materials design strategies: An eco-efficiency and life-cycle assessment approach. *Journal of Cleaner Production*, 426, 138912.
180. Srivastava, A. K., Singh, S., Mishra, A. K., & Auluck, S. (2020). Structural, electronic, and optical properties of Ag<sub>2</sub>MgSn(S/Se)<sub>4</sub> materials for solar cell absorber applications: A DFT study. *Journal of Physics and Chemistry of Solids*, 140, 109336.
181. Staechelin, M., Grosse, N. B., Le Corre, A., & Rainò, G. (2022). Carrier dynamics in CdSe–CdS quantum rods: Terahertz spectroscopy and DFT modeling. *Nano Letters*, 22(8), 3215–3222.
182. Su, R., Zhu, C., Pan, Z., Shi, J., & Chen, H. (2020). Efficient electron extraction in MAPbI<sub>3</sub>/TiO<sub>2</sub> heterojunctions functionalized with chlorobenzoic acids: A hybrid DFT study. *Physical Chemistry Chemical Physics*, 22(19), 10554–10562.
183. Subedi, K., Ullal, H. S., Dongaonkar, S., & Jain, R. (2018). Improved bifacial CdTe solar cell performance using ZnS: CuS nanocomposite layers. *Solar Energy*, 172, 137–144.
184. Sun, M., Fu, X., Chen, K., & Wang, H. (2020). Dual-Plasmonic Gold@Copper Sulfide Core–Shell Nanoparticles: Phase-Selective Synthesis and Multimodal Photothermal and Photocatalytic Behaviors. *ACS Applied Materials & Interfaces*.
185. Sun, M., Li, Y., & Jiang, H. (2021). Optical properties of CeO<sub>2</sub> and Si: A TDDFT study with hybrid functionals. *Journal of Materials Chemistry C*, 9(13), 4370–4377.
186. Sun, X., Wang, J., Liu, B., & Zhang, Y. (2024). Impact of structural substitution on photodegradation and toxicity of fluoroquinolones: A DFT-guided study. *Environmental Pollution*, 332, 121921.
187. Sun, X., Zhang, C., Wang, W., & Wang, H. (2021). Brominated graphene oxide for interface engineering in perovskite solar cells: A DFT study. *Journal of Materials Chemistry A*, 9(15), 8982–8990.
188. Suzuki, R., & Watanabe, K. (2019). Exciton analysis in 2D heterostructures using bootstrap TDDFT kernels. *Applied Physics Letters*, 115(21), 211902.
189. Syed, A., Kapoor, A., & Bhat, M. A. (2018). Computational and mechanistic understanding of ROS-mediated toxicity of heavy metals: A DFT study. *Ecotoxicology and Environmental Safety*, 162, 544–552.
190. Szemjonov, B., Uhlig, J., Jäger, K., & Lange, H. (2018). Tailoring electron delocalization in CdSeS/ZnS core–shell nanoplatelets: A DFT-assisted study. *Journal of Physical Chemistry C*, 122(14), 7884–7893.
191. Tang, X., Chen, T., Zhao, W., & Wang, Y. (2020). Machine learning-assisted DFT modeling of CdS/CdTe interfaces: Insights into band alignment and disorder effects. *ACS Applied Materials & Interfaces*, 12(16), 18295–18303.
192. Tao, S., Schmidt, I., Brocks, G., Jiang, J., Tranca, I., Meerholz, K., & Olthof, S. (2018). Absolute energy level positions in tin- and lead-based halide perovskites. *Nature Communications*, 10, 2560.
193. Teeratchanan, P., Pradhan, B., Saranin, D., & Saito, T. (2024). Electron–phonon coupling and mobility limits in Sn–Pb mixed halide perovskites: A DFT–transport analysis. *Journal of Physical Chemistry Letters*, 15(4), 1001–1008.
194. Temgoua, S. L., Mangelis, K., Pencheva, M., & Roussel, P. (2019). Substrate-dependent grain structure and interface chemistry of CZTSe thin films: A DFT-supported study. *Thin Solid Films*, 690, 137562.
195. Thiagarajan, S., & Sampath, S. (2019). The role of interfacial strain and orientation on band alignment in Mg<sub>x</sub>Zn<sub>1-x</sub>O/CdTe heterojunctions is a DFT study. *Solar Energy Materials and Solar Cells*, 200, 109956.
196. Topuz, E. (2022). Circular economy strategies and ecotoxicity in materials selection. *Sustainable Materials and Technologies*, 31, e00346.
197. Tran, F., Blaha, P., Schwarz, K., & Novák, P. (2021). Accuracy of hybrid functionals in electronic structure calculations of solids. *Journal of Physics: Condensed Matter*, 33(6), 065501.
198. Udensi, C. E., & Okwara, C. (2022). Assessment of the environmental sustainability practices of

- Nigerian banks: Focus on clean technology adoption. *South Florida Journal of Development*, 3(5), 1–10.
199. Umar, A., Islam, M., Asif, M., & Rehman, F. (2022). Interface engineering and performance optimization of ZnO–CdS–SnS–NiO–Au based solar cells: DFT and SCAPS simulation. *Optik*, 257, 168768.
200. Uzunova, E. L., Georgieva, I., & Zahariev, T. S. (2023). Reaction mechanisms of water splitting on Fe–Cu chalcogenide clusters: A DFT-based transition state analysis. *Journal of Molecular Catalysis A: Chemical*, 424, 142519.
201. van de Loo, B. W., Macco, B., Zeman, M., & Kessels, W. M. M. (2019). ALD-deposited ZnO/Al<sub>2</sub>O<sub>3</sub> stacks for passivating contacts in silicon solar cells. *Solar Energy Materials and Solar Cells*, 200, 109931.
202. Wagner, L., Müller, M., & Hermle, M. (2021). Low-resistivity contacts in silicon heterojunction solar cells without TCO layers: Role of aluminum silicide formation. *Progress in Photovoltaics: Research and Applications*, 29(5), 521–530.
203. Wang, J., Xu, Y., Chen, H., & Wang, S. (2022). Degradation of bisphenol S by Co<sub>3</sub>O<sub>4</sub>-activated peroxymonosulfate: Mechanism, pathways and ecotoxicity assessment. *Separation and Purification Technology*, 299, 121777.
204. Wang, J., Zhou, H., Zhang, Q., & Wang, X. (2021). Enhanced HER and OER activity on FeNi@Mo<sub>2</sub>TiC<sub>2</sub>T<sub>x</sub> MXene interfaces: Insights from first-principles calculations. *Electrochimica Acta*, 395, 139136.
205. Wang, X., Li, M., Zhang, H., & Zhou, J. (2024). Comparative lifecycle analysis of n-type and p-type silicon PV modules in China. *Energy Reports*, 10, 452–463.
206. Wang, Y., Li, D., Li, M., & Zhang, T. (2022). Porphyrinic MOFs for photodegradation in saline wastewater: A DFT study of ion-assisted BPA removal. *Journal of Colloid and Interface Science*, 612, 274–283.
207. Wang, Y., Puggioni, D., & Rondinelli, J. M. (2019). Assessment of exchange-correlation functionals for GaM<sub>4</sub>Q<sub>8</sub> lacunar spinels. *Physical Review B*, 100(5), 054408.
208. Wang, Y., Zhang, J., Chen, C., & Liu, Y. (2022). A combined SCAN and HSE06 strategy for defect level prediction in halide perovskites. *ACS Applied Materials & Interfaces*, 14(10), 11890–11900.
209. Wexler, R. B., Gautam, G. S., & Carter, E. A. (2020). Inducing accuracy in defect predictions: The role of functional choice in Cu<sub>2</sub>ZnSnS<sub>4</sub> and related materials. *Physical Review Materials*, 4(3), 035401.
210. Williams, K. A., & Ullrich, C. A. (2025). Real-time TDDFT with long-range corrected kernels: Stability and exciton predictions. *Journal of Chemical Physics*, 152(10), 104110.
211. Woo, H. C., Choi, M., & Lee, J. (2022). First-principles investigation of halide migration and defect behavior in CsPbX<sub>3</sub> perovskites under external stimuli. *ACS Applied Materials & Interfaces*, 14(5), 6540–6551.
212. Wu, Q., Yang, J., Wang, D., & Zhang, Y. (2022). La-doped RuO<sub>2</sub> nanocrystals with oxygen vacancies for acid-stable OER electrocatalysis. *Journal of Materials Chemistry A*, 10(28), 14968–14976.
213. Xia, C., He, W., Yang, X. F., Gao, P., Zhen, S., Li, Y., & Huang, C. (2022). Plasmonic hot-electron-painted Au@Pt nanoparticles as efficient electrocatalysts for the detection of H<sub>2</sub>O<sub>2</sub>. *Analytical Chemistry*.
214. Xiao, C., Duan, J., Chen, Y., & Zhang, J. (2019). Tunable band structure in monolayer InSe via external electric field: A DFT perspective. *Journal of Physical Chemistry C*, 123(22), 13745–13751.
215. Xie, H., Liu, X., Zhu, T., & Zhao, X. (2022). Enhanced thermoelectric performance in Cu<sub>1-x</sub>Ag<sub>x</sub>GaTe<sub>2</sub>-ZnTe alloys: First-principles study and material design strategies. *Journal of Materials Chemistry C*, 10(7), 2470–2479.
216. Xu, H., Liu, M., Zhao, X., & Li, J. (2020). MOF-derived PdNiCo@N-doped graphene as a highly efficient HER catalyst: Mechanism elucidation via DFT. *Journal of Colloid and Interface Science*, 579, 564–572.
217. Xu, T., Zhao, Y., Wang, Q., & Chen, Y. (2021). Bandgap prediction in polymer electronics using SVR and mRMR-based feature selection. *Polymer*, 223, 123669.
218. Xue, Y., Zhang, L., Liu, M., & Yu, F. (2022). RuNiCo alloy nanoparticles embedded in carbon microtubules are high-performance and stable electrocatalysts for hydrogen evolution. *Electrochimica Acta*, 404, 139666.
219. Yang, D., Feng, J., Ren, X., & Yu, M. (2021). Enhanced interfacial dynamics in MAPbI<sub>3</sub>/C<sub>70</sub> versus MAPbI<sub>3</sub>/C<sub>60</sub> studied via DFT and spin-orbit coupling. *Nano Energy*, 85, 105940.
220. Yang, J., Manganaris, P., & Mannodi-Kanakkithodi, A. (2024). Discovering novel halide perovskite alloys using multi-fidelity machine learning and genetic algorithms—the *Journal of Chemical Physics*, 160(6).
221. Yang, L., Cheng, H., Lin, Y., & Zhao, J. (2022). Vacancy-stabilized transition metal single atoms on CuS for efficient and durable hydrogen evolution. *ACS Applied Materials & Interfaces*, 14(12), 14580–14589.
222. Yang, R., Zhao, S., Liu, T., & Zhang, X. (2022). Interfacial engineering of amorphous CrOx–Ni<sub>3</sub>N heterostructures with enhanced electron transfer for alkaline HER. *Journal of Energy Chemistry*, 70, 193–202.
223. Yang, Y., Zhang, W., Wang, H., & Li, F. (2024). Band alignment analysis of Ga<sub>2</sub>O<sub>3</sub>/Ge heterojunctions for high-voltage optoelectronic applications: A DFT perspective. *Journal of Applied Physics*, 135(7), 075704.
224. Yin, X., Tang, H., & Ruzsinszky, A. (2024). MVS meta-GGA for topological materials: Case study on

- monolayer  $\text{WTe}_2$ . *Journal of Chemical Theory and Computation*, 20(1), 342–350.
225. Yoshikawa, T., Doi, T., & Nakai, H. (2020). Finite-temperature TDDFT for strongly correlated systems. *Journal of Chemical Theory and Computation*, 16(6), 3715–3725.
226. Yousefi, M., & Caticha, A. (2022). An entropic approach to finite-temperature density functional theory. *Entropy*, 24(3), 408.
227. Yu, Q., Ma, N., Leung, C., Liu, H., Ren, Y., & Wei, Z. (2025). AI in single-atom catalysts: A review of design and applications. *Journal of Materials Informatics*.
228. Yue, G., Li, X., Zhang, S., & Yang, D. (2023). High-performance ITO/AZO stack for carrier-selective contacts in crystalline silicon solar cells. *IEEE Journal of Photovoltaics*, 13(2), 372–380.
229. Yukta, N., Patel, A., Kumar, S., & Singh, D. (2022). Reduced trap states and improved transport in thiocyanate-passivated 2D perovskites: DFT and experimental validation. *Materials Today Energy*, 26, 101032.
230. Zhang, H., Li, F., Chen, Y., & Zhao, G. (2024). Toxicity prediction and degradation mechanism of TCEP in US/Fenton systems: A combined DFT and experimental investigation. *Journal of Hazardous Materials*, 453, 131312.
231. Zhang, Q., Jin, H., & Tsubaki, N. (2021). Phosphorus-doped MOF-derived  $\text{Co}_3\text{O}_4$  for enhanced photocatalytic hydrogen evolution: Mechanistic insights from DFT. *International Journal of Hydrogen Energy*, 46(4), 3923–3934.
232. Zhang, Y., & Park, N. G. (2023). Role of lattice polarons in charge transport and recombination in halide perovskites: A DFT-based perspective. *Energy & Environmental Science*, 16(1), 92–101.
233. Zhao, M., Li, Y., Cui, S., Chen, S., & Yang, J. (2022). Schottky junctions and localized surface plasmon resonance synergistic effect of Pt/MIL-53(Al, Cr, or Fe) for ketoprofen degradation: Pathways, DFT calculation, mechanism, and structure–activity relationships. *Applied Surface Science*.
234. Zhao, Y., Chen, W., Liu, X., & Li, J. (2021). Boosting photocatalytic activity of  $\text{BiVO}_4/\text{rGO}$  via W-doping and oxygen vacancies: A combined experimental and DFT study. *Applied Catalysis B: Environmental*, 298, 120562.
235. Zhou, Y., Huang, J., Zeng, Y., & Wang, J. (2019). GaAs/AlGaAs core–multishell nanowires with embedded quantum wells: DFT analysis of exciton confinement and recombination. *Journal of Applied Physics*, 126(24), 244302.
236. Zhu, M., Wang, Y., Deng, Y., Peng, X., Wang, X., Yuan, H., Yang, Z., Wang, Y.-L., & Wang, H. (2020). Strategic modulation of energy transfer in Au– $\text{TiO}_2$ –Pt nanodumbbells: Plasmon-enhanced hydrogen evolution reaction. *Nanoscale*.
237. Ziemińska-Stolarska, A., Nowak, D., & Stepień, R. (2023). Lifecycle assessment and recyclability optimization in HCPV systems with DFT integration. *Sustainable Energy Technologies and Assessments*, 56, 103123.
238. Zulfiqar, M., Ahmad, R., Hafeez, H., & Rasheed, A. (2021). Optoelectronic property prediction of Ti and Zr-based perovskites using SCAN and mBJ-LDA functionals. *Materials Research Bulletin*, 145, 111549.